

# Neural models of multiscale systems: conceptual limitations, stochastic parametrizations, and a climate application

Fabrizio Falasca\*

*Courant Institute of Mathematical Sciences  
New York University, New York, NY, USA*

(Dated: July 1, 2025)

This work explores key conceptual limitations in data-driven modeling of multiscale dynamical systems, focusing on neural emulators and stochastic climate modeling. A skillful climate model should capture both stationary statistics and responses to external perturbations. While current autoregressive neural models often reproduce the former, they typically struggle with the latter. We begin by analyzing a low-dimensional dynamical system to expose, by analogy, fundamental limitations that persist in high-dimensional settings. Specifically, we construct neural stochastic models under two scenarios: one where the full state vector is observed, and another with only partial observations (i.e. a subset of variables). In the first case, the models accurately capture both equilibrium statistics and forced responses in ensemble mean and variance. In the more realistic case of partial observations, two key challenges emerge: (i) identifying the *proper* variables to model, and (ii) parameterizing the influence of unobserved degrees of freedom. These issues are not specific to neural networks but reflect fundamental limitations of data-driven modeling and the need to target the slow dynamics of the system. We argue that physically grounded strategies – such as coarse-graining and stochastic parameterizations – are critical, both conceptually and practically, for the skillful emulation of complex systems like the coupled climate system. Building on these insights, we turn to a more realistic application: a stochastic reduced neural model of the sea surface temperature field and the net radiative flux at the top of the atmosphere, assessing its stationary statistics, response to temperature forcing, and interpretability.

## CONTENTS

I. Introduction	2
II. Theoretical Framework: Data-driven stochastic climate modeling and response theory	4
A. Reduced stochastic models: theoretical and practical considerations	4
B. Response theory: a (very) brief overview	5
III. Limitations of data-driven modeling by analogy: the case of partial observations	7
A. A triad model as a prototype stochastic climate model	7
B. Data-driven modeling when we observe the full state vector	7
1. Functional form of the data-driven models considered	8
2. Stationary statistics	8
3. Response of probability distributions to <i>external</i> perturbations	8
4. Main takeaways	10
C. Data-driven modeling when we do not observe the full state vector	11
1. Functional form of the reduced order models considered	11
2. Stationary and perturbed statistics of the scalar model	12
3. Main takeaways	13
IV. A real-world example: radiative responses to temperature perturbations in a climate model	14
A. Scientific problem at hand	14
B. A reduced order model of surface temperature and radiative fluxes	15
1. Data, preprocessing and coarse-graining	15
2. Stationary statistics and forced responses	16
3. Interpretability and understanding	18
4. Main takeaways	19

---

\* fabri.falasca@nyu.edu

V. Conclusions	20
A. Technical and practical details on the model formulations	21
1. Multivariate data-driven stochastic models	21
2. Scalar data-driven stochastic models	22
Acknowledgments	22
References	23

## I. INTRODUCTION

A key challenge in current applied mathematics is to build data-driven models from partial observations of complex physical systems. Among the most challenging examples is the climate system: a forced, dissipative, and chaotic system whose dynamics span at least 15 orders of magnitude across spatial and temporal scales [1]. This problem has been extensively studied over the past three decades, mainly in the realm of reduced-order models [2]. Seminal contributions include the work of Penland and collaborators [3–5], the multilevel modeling strategies of Kravtsov and colleagues [6–9], and the contributions of Majda et al. [10, 11]. More recent proposals also include dynamical Markov-chain models to simulate the evolution of probability distributions as in [12–14] as well as novel ideas from generative models [15].

Recently, autoregressive models based on deep learning architectures have been proposed as potential *emulators* of the weather [16–18] and climate [19–25] systems. These tools build on earlier efforts in data-driven reduced-order modeling by considering new powerful architectures (i.e. neural networks) and by attempting to simulate the system in its full complexity and dimensionality. For example, [24] and [25] respectively seek to emulate the full ocean and atmosphere components of two state-of-the-art climate models. These models often excel at reproducing stationary statistics and generating forecasts across a range of time horizons, marking a promising direction for computationally efficient climate modeling. However, neural network emulators also exhibit several limitations. Long trajectory roll-outs often suffer from error accumulation, which can drive the system toward instability. While promising approaches have been proposed to address this issue, e.g. [26, 27], these are currently research directions still to be explored across different models and scenarios. Instead current implementations maintain stability by prescribing part of the climate system as boundary conditions (e.g. [24] is an ocean emulator driven by pre-computed atmospheric fields as boundary conditions). We refer the reader to Pedersen et al. [26] for a detailed discussion of the stability challenges in autoregressive modeling. An additional issue, relevant for this study, is that skill in capturing unforced variability may not always guarantee accurate responses in perturbation experiments, limiting their use for causal mechanistic studies of climate dynamics. This leads to two important consequences: neural emulators (i) usually do not generalize in out-of-distribution climate change experiments and (ii) they may often not capture the right causal relations across variables. Note that the two issues (i) and (ii) above are likely related. The work of Van Loon et al. [28] provides us with a clear and insightful example of this limitation in the context of the “pattern effect” problem [29, 30], i.e. the influence of sea surface temperature (SST) warming patterns on the Earth’s energy imbalance. Van Loon et al. [28] considered the ACE2 emulator [21] and built a Green’s function by iteratively applying warming perturbations in different locations in the sea surface temperature (SST) field and computing the responses in the radiative flux at the top of the atmosphere (TOA). In doing so, [28] showed how such Green’s function does not capture in a quantitative way the causal relations between the SST and the radiative fluxes. This is just one example of the limitations of neural emulators in capturing responses to perturbations. Even if such issues are addressed in specific cases, they highlight a broader challenge: building general-purpose emulators that reliably capture forced responses remains inherently difficult and context-dependent. Other examples related to capturing forced responses to changes in the boundary conditions can be found in [24, 25]. Additionally, we note that current emulators usually focus on one climate component at a time, ocean or atmosphere, and the challenges described above, and also later in this paper, are expected to get worse when a fully coupled system will be considered. In general, limitations of neural emulators in capturing responses to external perturbations imply that such tools may not be yet ready to explore causal questions in climate dynamics.

While the field of neural emulation is advancing rapidly, it is useful to step back and examine its fundamental limitations in capturing forced responses, both from a theoretical standpoint and in controlled settings. In the first part of this paper, we build on a series of previous works by A. Vulpiani and collaborators on the limitations of data-driven modeling [31–33]. We analyze a simplified stochastic dynamical system to illustrate fundamental limitations

that are expected to persist in high-dimensional settings. Specifically, we ask the following question: *Can neural autoregressive models, trained on (practically) infinitely long time series, accurately capture the response to general external perturbations?* In addressing this question, we consider two scenarios:

- *Fully observed state vector.* Data-driven modeling when the entire state vector is available. Here, we assume no knowledge of the underlying equations, but we have access to very long time series of the complete system state vector.
- *Partially observed state vector.* Data-driven modeling in the presence of partial observations. This reflects common constraints in modeling high-dimensional systems from data, where the full set of relevant variables is typically unknown. In this more realistic setting, we again assume no knowledge of the underlying equations and only partial access to the system’s state vector.

To tackle such questions we proceed pedagogically by focusing on a “triad model” first proposed by Majda and collaborators in [34] and used as a testbed for Fluctuation-Dissipation theorem strategies in [35, 36]. The model mimics the abstract structure of dynamical cores in large-scale climate models with dynamics characterized by a linear operator and an energy conserving nonlinear, quadratic operator. We address the questions above by training neural stochastic emulators on a long integration of the triad model and test the models’ performance on stationary and perturbed cases. In doing so, we face the following issue: quantifying how an emulator respond to general forcing is an ill-posed question, as there are infinite possible forcings. Nonetheless, the linear response to a general forcing can be computed by convolving the forcing with an impulse response operator [37, 38]. Such operator can be retrieved from the model, and is here considered as the *building block* to get right for an emulator to, at least, capture the linear part of the response to general external perturbations. In the case of a fully observed state vector we show that the inferred neural model is able to reproduce stationary statistics of the system, i.e. the probability distributions and autocorrelation functions, as well as the response to small external perturbations. Therefore, there is no fundamental limitation for a neural model to respond to external perturbation, i.e. shifts in the input distribution, at least for perturbations of small amplitudes. However, in the case of partial observations, as in more realistic settings, we argue how the performance of a data-driven model necessarily depends on (i) the choice of variables to model and (ii) how to parametrize the unobserved degrees of freedom. The field of reduced order modeling, introduced earlier, has long sought to confront these challenges by formulating effective Langevin equations capturing the coarse-grained, slow dynamics of the system [5, 39–41]. Therefore, we will argue that a promising perspective is to build on such established approaches, emphasizing coarse-grained dynamics and stochastic parameterizations, while using neural networks as powerful tools within this framework, rather than as wholesale replacements.

We emphasize that the focus on a simplified dynamical system is not a limitation in this context. In fact, the goal is not to demonstrate the success of a method, but to illustrate, by analogy, fundamental issues that are already evident in low dimensions and are likely to become more pronounced in higher-dimensional settings. As Smith (2002) [42] argues, while it is unreasonable to expect solutions to low-dimensional problems to generalize to high dimensions, so too it is unlikely that limitations observed in low-dimensional systems will vanish in high-dimensional, operational models.

Building on these ideas, we conclude this study by considering a real-world example. Throughout this paper, we emphasize, where possible, the distinction between “real-world examples/systems” and merely high-dimensional dynamics. By real-world examples we refer to situations where (i) we observe only the temporal evolution of a subset of variables without access to the full state vector (i.e. a projection of the full dynamics) or (ii) where even in the presence of all variables the system encompasses a huge number of spatial and temporal scales (as for the climate and weather system). Both cases (i) and (ii) lead to the need to formulate *effective* rather than *primitive* equations for both practical and conceptual reasons [40]. For an early instance of case (ii), see the work of Charney (1948) [43], Charney et al. (1950) [44] and the discussion in Dalmedico (2001) [41]. The example we consider simulates the joint evolution of the sea surface temperature (SST) field and the net radiative flux at the top of the atmosphere (TOA). Our motivation lies in understanding the spatial structure of climate feedbacks by addressing the so-called pattern effect, i.e. the dependence of Earth’s energy imbalance on the spatial patterns of surface warming [30]. To this end, we develop a simplified stochastic neural model based on 20 SST modes and a global mean, scalar time series for the radiative flux. Unobserved degrees of freedom are parametrized through multiplicative (state-dependent) noise. We demonstrate that the model captures both the stationary statistics and the radiative fluxes response to imposed temperature perturbations in two climate change experiments. Such model can then be used to explore the linkages between surface temperature warming patterns and radiative fluxes, as well as a “reconstruction” tool, by predicting the change in one variable given prescribed changes in the other. Finally, we apply ideas from response theory to infer *direct* causal relationships between surface temperature and TOA radiative flux. These results show qualitative agreement with perturbation experiments using atmospheric-only climate models and align with current physical

understanding of radiative feedbacks in the climate system.

The paper is organized as follows: in Section II we introduce the theoretical ideas underpinning this work. In Section III we discuss key conceptual difficulties in data-driven modeling of real-world dynamical systems. In Section IV we present a real-world application by focusing on radiative feedbacks to temperature perturbations. Conclusions then follow in Section V.

## II. THEORETICAL FRAMEWORK: DATA-DRIVEN STOCHASTIC CLIMATE MODELING AND RESPONSE THEORY

We begin by outlining the main theoretical concepts that underpin this work. First, we briefly introduce general ideas for constructing Langevin-like equations from partial observations of multiscale systems. We then review key aspects of response theory, which offers a general framework for understanding and assessing the ability of models to respond to perturbations.

### A. Reduced stochastic models: theoretical and practical considerations

*a. Why reduced order modeling and effective equations?* Consider a nonlinear dynamical system  $\dot{\mathbf{x}} = \mathbf{f}(\mathbf{x})$ . The main interest in data-driven modeling, is to estimate the operator  $\mathbf{f}$  directly from data. In doing so we face a serious limitation: in many high-dimensional complex systems we have access only to partial observations of the state vector  $\mathbf{x}$ . A temptation could be to use Taken’s embedding theorem [45]. While theoretically appealing, this strategy has significant practical limitations: it is not valid for stochastic systems and it becomes infeasible as the dimensionality of the system increases [32, 33, 40, 46–48]. A more promising direction leverages the multiscale nature of real-world dynamical systems by focusing on coarse-grained, *effective* dynamics. In some cases, it is possible to identify slow variables exhibiting low-dimensional effective dynamics and treat the cumulative effect of unresolved fast variables on the slow ones as stochastic forcing terms [2–4, 36, 37, 49–52]. In these cases, the system state vector  $\mathbf{x}$  can be decomposed into slow and fast components,  $\mathbf{x} = (\mathbf{x}_s, \mathbf{x}_f)$ , and motivates the derivation of an effective Langevin equation for the slow variables of the form:

$$d\mathbf{x}_s = \mathbf{f}_{eff}(\mathbf{x}_s)dt + \mathbf{\Sigma}(\mathbf{x}_s)d\mathbf{W}, \quad (1)$$

where  $\mathbf{f}_{eff}$  represents the deterministic “drift” dynamics,  $\mathbf{x}_s$  are the slow variables and  $\mathbf{W}$  is the standard Wiener process. The noise term parametrizes the cumulative effect of unresolved fast processes  $\mathbf{x}_f$  on the slow ones. In the general case the noise is “multiplicative”, i.e. state dependent:  $\mathbf{\Sigma}(\mathbf{x}_s)$ . However, in many practical applications, additive noise can be preferred, with  $\mathbf{\Sigma}$  independent of  $\mathbf{x}_s$ . In what follows, we will simplify notation by referring to  $\mathbf{x}$  instead of  $\mathbf{x}_s$ , and we will clarify the precise meaning as needed in the text.

The reduced-order modeling approach emerges naturally in the study of large-scale climate dynamics, where recurrent spatiotemporal patterns, i.e. modes of variability, dominate the system’s behavior [53, 54]. Unlike traditional general circulation models (GCMs) that aim to simulate as many spatiotemporal scales as possible, reduced models target specific processes/problems, capturing a few key degrees of freedom while treating the rest as stochastic forcing. This not only reduces computational cost but also enhances mechanistic understanding, by isolating core processes and studying their qualitative behavior (see e.g. [55], as well as the introduction of [44]). Consequently, there is a growing need for systematic methods to reduce the dimensionality of high-dimensional systems and to quantify causal interactions across their degrees of freedom. This has fueled the development of low-dimensional stochastic models learned either from data [2–4, 7, 10, 51, 56] or from known equations [49, 50, 57, 58], as well as inference-based techniques to infer interactions across modes of variability [59–62]. In this paper, we will primarily focus on data-driven stochastic modeling from partial observations. Nevertheless, we emphasize that even when all the relevant variables of the system are known, in multiscale physical systems there is often a need to formulate new effective (even deterministic) equations of the slow variables rather than focusing on the primitive equations. A classic example in the weather/climate literature is given by Charney (1948,1949) [43, 63] as well as Charney et al. (1950) [44]. Charney was among the first to recognize the importance of filtering out what he termed “meteorologically insignificant noise” from the primitive equations, leading to more interpretable and computationally efficient effective equations.

*b. Data-driven reduced-order modeling: practical considerations and prior work.* In practice, given a phenomenon of interest, we typically begin with spatiotemporal data consisting of  $N$  time series of length  $T$ . We then often proceed as follows:

- *Coarse-grained dynamics.* In spatiotemporal systems like climate, coarse-graining involves: (i) selecting a few relevant modes, (ii) isolating specific temporal scales, and (iii) choosing a limited set of variables. Regarding point (i), we reduce the dimensionality of the system in terms of some bases, a common choice is the one of Empirical Orthogonal Functions (EOFs) [8, 39]. We retain only the first  $n < N$  of such bases, and project the data onto them to obtain the principal components (PCs), which serve as the reduced time series for model training. Although EOFs are convenient, they may not be always optimal, and alternatives such as those in [62, 64, 65] (among many others) may be more suitable depending on the application. The performance of the final model is sensitive to all coarse-graining choices (i–iii); see, e.g., [66, 67]. Considering the “right” coarse-grained procedures is perhaps the most difficult step in modeling from data. There is in fact no general mathematical guideline in high-dimensional dynamical systems for choosing the *proper* variables to model, an old problem [68] emphasized in many new contributions, such as [31, 47, 48, 69].
- *Inferring a stochastic model.* Given a reduced order representation of the system, we are now left with the task of inferring a stochastic model of the form of Eq. (1). Many studies have shown that, for specific observables (e.g., sea surface temperature anomalies), a linear drift with additive noise provides forecasting skill comparable to full complexity models [4, 5, 70, 71]. This leads to a Linear Inverse Model (LIM) [3] of the form

$$d\mathbf{x} = \mathbf{L}\mathbf{x}dt + \mathbf{\Sigma}d\mathbf{W},$$

where  $\mathbf{L}$  is a linear operator,  $\mathbf{\Sigma}$  is a noise matrix and  $\mathbf{W}$  is the standard Wiener process. An interesting recent extension to tackle colored noise can be found in [72]. The multilevel regression proposed by Kratsov et al. (2005) [6, 7] generalizes these ideas by incorporating quadratic nonlinearities and non-Markovian effects with a series of “matryoshka”-like levels for residuals. In many practical cases, however, temporal coarse-graining (e.g., averaging over a few time steps) can effectively remove memory effects, allowing a Markovian closure [73]. In the framework proposed in [6, 7], the drift consists of both linear and quadratic nonlinear components. The inclusion of quadratic nonlinearities is physically motivated rather than ad-hoc. As shown in Section 2 of Lorenz (1963) [74], projecting forced-dissipative flows (in periodic domains) onto Fourier modes, yield a set of infinite coupled ODEs with linear and quadratic interactions for the modes’ amplitudes. In particular, the quadratic nonlinearity  $\mathbf{B}(\mathbf{x}, \mathbf{x})$  should be energy-conserving, satisfying  $\mathbf{x} \cdot \mathbf{B}(\mathbf{x}, \mathbf{x}) = 0$ . This abstract representation underlies the starting point of the Majda-Timofeyev-Vanden Eijnden (MTV) mode reduction framework [49, 50, 57, 58]. Additionally, Majda and Harlim focused on the energy conservation constraint above to propose physically constrained regression models [11]. Guided by these insights, the neural models proposed in this work will have a deterministic dynamics specified by a linear term  $\mathbf{L}$  and general nonlinear terms  $\mathbf{n}(\mathbf{x})$ ; in formulae:

$$\frac{d\mathbf{x}}{dt} = \mathbf{L}\mathbf{x} + \mathbf{n}(\mathbf{x}).$$

It is in fact a sensible choice to guide the learning by specifying a decomposition into linear and nonlinear terms, instead of letting the neural network “figure out” the functional form by itself (see also [75]). Furthermore, we will move beyond additive noise and incorporate multiplicative (state-dependent) noise, both in one and higher dimensions. As we will show, incorporating state-dependent noise can be at times critical for accurately capturing the system’s response to external perturbations in the presence of partial observations.

## B. Response theory: a (very) brief overview

In this paper, we argue that a reduced-order model should capture not only the system’s stationary statistics but also its response to external perturbations. This naturally raises the question: *How to assess skillful responses to general perturbations?* Since it is impossible to test responses to the full space of possible forcings, linear response theory provides a principled framework for analyzing the system’s linear response to perturbations.

*a. Impulse response operator.* Given a  $n$ -dimensional coarse-grained state vector  $\mathbf{x}(t) = [x_1, x_2, \dots, x_n](t)$ , we perturb a degree of freedom  $x_j$  with a small, step function perturbation  $x_j(0) \rightarrow x_j(0) + \delta x_j(t)$ , with  $\delta x_j(t) = \Delta_j \delta(t)$ , where  $\delta(t)$  is a delta function and  $\Delta_j$  is a small perturbation amplitude [47, 76]. We then consider a general observable  $A(x_k(t))$  (i.e. a general functional of the system) and quantify its response, in terms of ensemble average, as:

$$\delta \langle A(x_k(t)) \rangle = \langle A(x_k(t)) \rangle_p - \langle A(x_k(t)) \rangle, \quad (2)$$

where  $\langle \cdot \rangle$  refers to ensemble average and the subscript “p” refers to the perturbed system. In this paper we are going to focus on two different specific observables: (i)  $A(x_k(t)) = x_k(t)$  and (ii)  $A(x_k(t)) = (x_k(t) - \mu_k(t))^2$ , with  $\mu(t)$  representing the time-dependent mean of the perturbed distribution. The two observables allow us to capture time-dependent responses in the mean and variance of the perturbed distribution respectively. The impulse response operator  $\mathbf{R}(t) \in \mathbb{R}^{n,n}$  is then defined as:

$$R_{k,j}(t) = \lim_{\delta x_j(0) \rightarrow 0} \frac{\delta \langle A(x_k(t)) \rangle}{\delta x_j(0)}. \quad (3)$$

The utility of the inferred impulse response operator is two-fold:

- *Causal inference.* Understanding causal relations across degrees of freedoms in physical systems require us to study the effect of interventions on the system [77]. The inferred response operator quantifies time-dependent cause-effect dependencies across degrees of freedoms  $x_j$  and  $x_k$ ; under the assumption that the reduced order models correctly capture the physics of the system. For more details to this physics-based approach to causal inference see [47, 62, 78–80].
- *Response to generic time-dependent forcing.* The response operator  $\mathbf{R}(t)$  can be used to predict the response of the system to small, but general, time-dependent external forcing  $\mathbf{f}(t) \in \mathbb{R}^N$  applied directly to the system’s degrees of freedoms as:

$$\delta \langle A(x_k(t)) \rangle = \sum_j \int_0^t R_{k,j}(\tau) f_j(t - \tau) d\tau. \quad (4)$$

Importantly, while we assume linearity in the system’s response, the formulas above are valid for both linear and nonlinear systems.

A data-driven model capable of accurately capturing the impulse response operator will also capture the time-dependent causal interactions across degrees of freedom. Response theory can then be used to assess the skills of emulators by going beyond purely statistical metrics such as r-squared, by for example assessing the causal sensitivity of the system to external perturbation, see e.g. discussion in Falasca et al. (2024) [62]. Since the linear response to small perturbations is given by the convolution formula in Eq. (4), recovering the impulse response operator ensures a faithful approximation of the system’s linear response to general forcings. For this reason, we view the impulse response operator as a fundamental *building block* that a data-driven model must reproduce to reliably capture at least the linear component of responses to general perturbations, and is necessary (but not sufficient) to capture nonlinear responses as well.

*b. Inferring the response operator in practice.* Given a model  $d\mathbf{x} = \mathbf{f}(\mathbf{x})dt + \Sigma(\mathbf{x})d\mathbf{W}$  we build the impulse response operator as follows:

1. We simulate a very long trajectory of the model, starting from a random initial condition and remove an initial transient. We then sample  $N_e$  random points from the simulation to define an ensemble of  $N_e$  initial conditions on the model’s attractor.  $N_e$  should be very large (i.e.  $N_e \gg 1$ ) in order to sample the whole attractor.
2. For each one of the  $N_e$  initial conditions, we impose an impulse perturbation  $x_j(0) \rightarrow x_j(0) + \Delta_j \delta(t)$  of size  $\Delta_j$  on the  $j$ -th degree of freedom at time  $t = 0$ .  $\delta(t)$  is the Dirac delta function. The amplitude  $\Delta_j$  should be theoretically infinitesimally small. In practice we do as follows: we consider the long time series of  $x_j(t)$  from the long control integration above and define  $\Delta_j = 10^{-2} \sigma_j$ , where  $\sigma_j$  is the standard deviation of time series  $x_j(t)$ .
3. Therefore, for a given initial condition  $\mathbf{x}(0)$ , we simulate two trajectories: a control trajectory without perturbation and a perturbed one, where an impulse perturbation  $\Delta_j$  has been imposed on the  $j$ -th degree of freedom at time  $t = 0$ . This procedure is repeated in parallel for all initial conditions, resulting in an ensemble of  $N_e$  paired of control and perturbed trajectories.
4. At each time  $t$  we then estimate the time dependent ensemble average  $\langle A(x_k(t)) \rangle$  of an observable  $A(x_k(t))$  for both the perturbed and unperturbed run. We refer to the perturbed and control ensemble average respectively as  $\langle A(x_k(t)) \rangle_p$  and  $\langle A(x_k(t)) \rangle_c$ . The observables considered in this study are going to be: (i)  $A(x_k(t)) = x_k(t)$  and (ii)  $A(x_k(t)) = (x_k(t) - \mu_k(t))^2$ , with  $\mu(t)$  representing the time-dependent mean of the perturbed distribution, therefore quantifying the response in ensemble mean and variance.

5. We define the impulse response operator for observable  $A(x_k(t))$  as

$$R_{k,j}(t) = \frac{\delta A(x_k(t))}{\Delta_j} = \frac{\langle A(x_k(t)) \rangle_P - \langle A(x_k(t)) \rangle}{\Delta_j}.$$

### III. LIMITATIONS OF DATA-DRIVEN MODELING BY ANALOGY: THE CASE OF PARTIAL OBSERVATIONS

As argued by Cecconi et al. (2012) [31], the main challenge in modeling real-world dynamical systems from data stems from their high dimensionality. Learning a dynamical system from data requires sufficiently long time series to sample many recurrences. However, the recurrence time, i.e. the time needed for a trajectory to return to a previous region in state space, scales exponentially with the system’s dimensionality [31, 81]. The success of data-driven methods in real-world systems is therefore often attributed to the presence of an *effective* low-dimensional dynamics. In other words, the dynamics of the system usually lives on a low-dimensional manifold embedded in a higher-dimensional space. This so-called “manifold hypothesis” underpins research in fields ranging from spatiotemporal chaos [82–85] to neuroscience [86–90], biophysics [91, 92], artificial neural networks [93, 94] and climate dynamics [1, 54, 74, 95, 96]. In practice, however, even when a system exhibits low effective dimensionality, we still face several difficult challenges. First, it is often unclear how to construct an optimal basis for efficient modeling in the system’s intrinsic coordinates [64]. Second, and more fundamentally, we typically observe only a subset of relevant variables of a complex, multiscale physical system. Here we illustrate how learning on only partial observations, as is common in real-world applications [10, 33], can hinder data-driven modeling, even when the underlying dynamics is low-dimensional and seemingly tractable. Importantly, while the discussion is framed in terms of neural emulators, motivated by current challenges in climate science, the issues we highlight are general and inherent to data-driven approaches for real-world dynamical systems.

#### A. A triad model as a prototype stochastic climate model

We consider a *triad model* originally introduced by Majda and collaborators in the context of low-frequency climate dynamics [34, 36]. The model is:

$$\begin{aligned} dx_1 &= (L_{11}x_1 + L_{12}x_2 + L_{13}x_3 + Ix_1x_2)dt \\ dx_2 &= (-L_{12}x_1 - Ix_1^2 - \gamma_2\epsilon^{-1}x_2)dt + \sigma_2\epsilon^{-1/2}dW_2 \\ dx_3 &= (-L_{13}x_1 - \gamma_3\epsilon^{-1}x_3)dt + \sigma_3\epsilon^{-1/2}dW_3 \end{aligned} \tag{5}$$

This idealized system mimics the functional structure of a reduced stochastic climate model, featuring linear couplings  $L_{11}, L_{12}, L_{13}$  and energy-conserving quadratic nonlinearities. The parameter  $I$  controls the strength of the nonlinearity: when  $I = 0$ , the model reduces to purely linear dynamics. The parameter  $\epsilon$  sets the time-scale separation between the slow mode  $x_1$  and the fast modes  $(x_2, x_3)$ , allowing exploration of multiscale dynamics in a controlled setting. The terms  $W_2$  and  $W_3$  represent independent Wiener processes, introducing stochastic forcing into the second and third equations. This stochastic forcing, together with the linear damping terms  $\gamma_2$  and  $\gamma_3$ , serves as a linear proxy for the nonlinear self-interactions of the fast variables (see Eq. (4) in [49] or Section 3.3 in [37] for further details). Importantly, the model generates relatively small, but significant, deviations from Gaussianity which is a relevant feature in the study of low-frequency climate dynamics [34] and found in both general circulation models and observational data, see e.g. [97–99].

#### B. Data-driven modeling when we observe the full state vector

We consider the relatively simple case of a low-dimensional dynamical system with only one characteristic time scale (i.e.  $\epsilon = 1$ ). The parameters chosen for this first test are:  $L_{11} = -2$ ,  $L_{12} = 1$ ,  $L_{13} = 1$ ,  $\gamma_2 = 0.6$ ,  $\gamma_3 = 0.4$ ,  $\sigma_2 = 1.2$ ,  $\sigma_3 = 0.8$ ,  $I = 1$ ,  $\epsilon = 1$ . We now integrate the system in (5) with an Euler–Maruyama scheme for a period of length  $T = 10^7$  with time step  $dt = 0.01$  (i.e.  $10^5$  Model Time Units). As we will show later, given the system’s decorrelation time scale, the resulting time series can be effectively treated as infinitely long. With this long trajectory of the full state vector  $\mathbf{x}(t) = [x_1, x_2, x_3](t)$  in hand, we now attempt to learn data-driven models directly from the time series. We construct both linear and nonlinear stochastic models. We specify the functional forms of these models and assess their ability to reproduce both the stationary and perturbed statistics of the original system defined in Equation (5).

### 1. Functional form of the data-driven models considered

We consider two data-driven models and report their functional forms below. To keep the main text focused, we leave the technical details of the fitting procedures, along with details of the neural networks, in Appendix A.

- *Linear model.* We consider the following linear model:

$$d\mathbf{x} = \mathbf{L}\mathbf{x}dt + \Sigma d\mathbf{W}, \quad (6)$$

$\mathbf{L}$  is a linear operator,  $\Sigma\Sigma^T$  is the noise covariance matrix and  $\mathbf{W}$  is the standard Wiener process.

- *Nonlinear model.* The nonlinear model takes the following form:

$$d\mathbf{x} = (\mathbf{L}\mathbf{x} + \mathbf{n}(\mathbf{x}))dt + \Sigma d\mathbf{W}. \quad (7)$$

$\mathbf{L}$  is a linear operator and  $\mathbf{n}(\mathbf{x})$  is parametrized by a Multilayer Perceptron (MLP). Crucially, the term  $(\mathbf{L} + \mathbf{n}(\mathbf{x}))$  is fitted jointly. As for the linear model, the  $\Sigma\Sigma^T$  is the noise covariance matrix and  $\mathbf{W}$  is the standard Wiener process. In what follows we are going to often refer to this model as “neural model” or “neural emulator”.

The two models above are trained on a long simulation of the triad system in Eq. (5).

Note that this is the only Section in this work where we compare linear and nonlinear autoregressive models. The linear method is considered for two reasons. First, we show that linear inverse modeling (LIM), as originally proposed in [3], serves as a strong baseline for neural autoregressive models, successfully capturing both the mean and variance of the system’s stationary distribution, the autocorrelation functions, and the ensemble-mean response to external perturbations. Second, and consistent with theoretical expectations [36], we demonstrate that linear models are fundamentally limited in capturing changes in the full probability distribution: for instance, they cannot represent any response in the variance to external forcings. This limitation restricts their usefulness for studying forced changes in distributions beyond the mean, which, dependent on the research question, can be a central objective in climate science.

### 2. Stationary statistics

We integrate the two data-driven models inferred from data and specified in Eq. (6) and (7) for  $T = 10^7$ , yielding time series of the same length as those obtained from the original triad system. We then compare the modeled and original probability density functions (PDFs) and autocorrelation functions (ACFs), as shown in Figure 1. The neural model described in Equation (7) successfully captures the stationary distributions of all three modes  $x_1(t)$ ,  $x_2(t)$  and  $x_3(t)$ . In particular, it outperforms the linear model by accurately reproducing the non-Gaussian features of the first mode  $x_1$ . Both models also reproduce the autocorrelation functions well, as seen in the second row of Figure 1. In summary, the neural emulator defined in Equation (7) is capable of capturing both the stationary statistics and temporal correlations of the full state vector  $\mathbf{x}(t)$ . At the same time, the linear model serves as a strong baseline for evaluating more sophisticated data-driven approaches.

### 3. Response of probability distributions to external perturbations

*a. Impulse response functions* We now examine the impulse response of the original triad model (Equation (5)), the linear model (Equation (6)), and the nonlinear neural model (Equation (7)). Specifically, we analyze the time-dependent response of observables  $A(x_k(t))$ , with  $k = 1, 2, 3$ , to an impulse perturbation imposed on  $x_1(0)$  at time  $t = 0$ . The observables considered here are the mean and variance of the time-dependent perturbed distribution. The ensemble size considered here is  $N_e = 10^5$  trajectories. The results, shown in Figure 2, reveal that the nonlinear neural model captures the mean response of the distribution quantitatively, while the linear model captures it only qualitatively. The most significant differences arise in the response of the variance: the linear model yields exactly zero variance response, clearly highlighting the limitations of linear dynamics. This is expected, as a linear model with a Gaussian invariant measure produces zero response to any quadratic functionals, such as the variance, consistent with the theoretical results in [36]. In contrast, the neural model captures the variance response with relatively high fidelity. As argued in Section II B, the impulse response operator plays a foundational role in determining a model’s ability to capture the linear part of the response to general perturbations. We therefore consider the neural model presented here as a skillful model both in terms of reproducing the stationary distribution as well as the response to forcing.



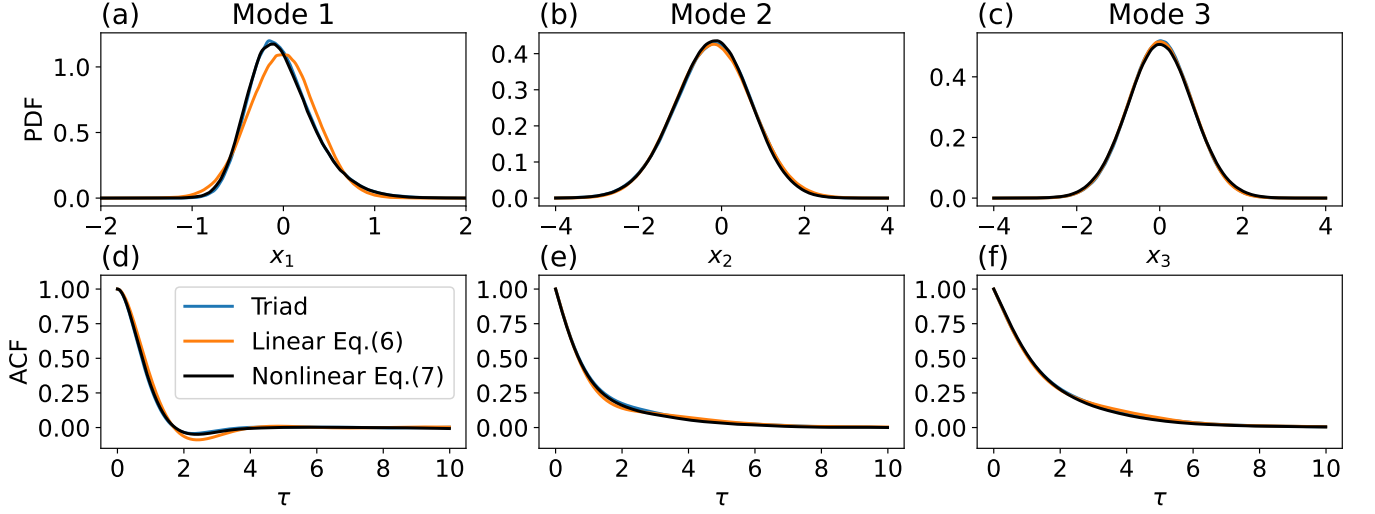


FIG. 1. First row: stationary distributions of the variables  $x_1(t)$ ,  $x_2(t)$  and  $x_3(t)$  as modeled by the original triad system in Eq. (5), the linear emulator in Eq. (6) and the neural emulator in Eq. (7). Stationary distributions are obtained after running the three systems for  $10^5$  model time units. Second row: same as the first row but for the autocorrelation functions.

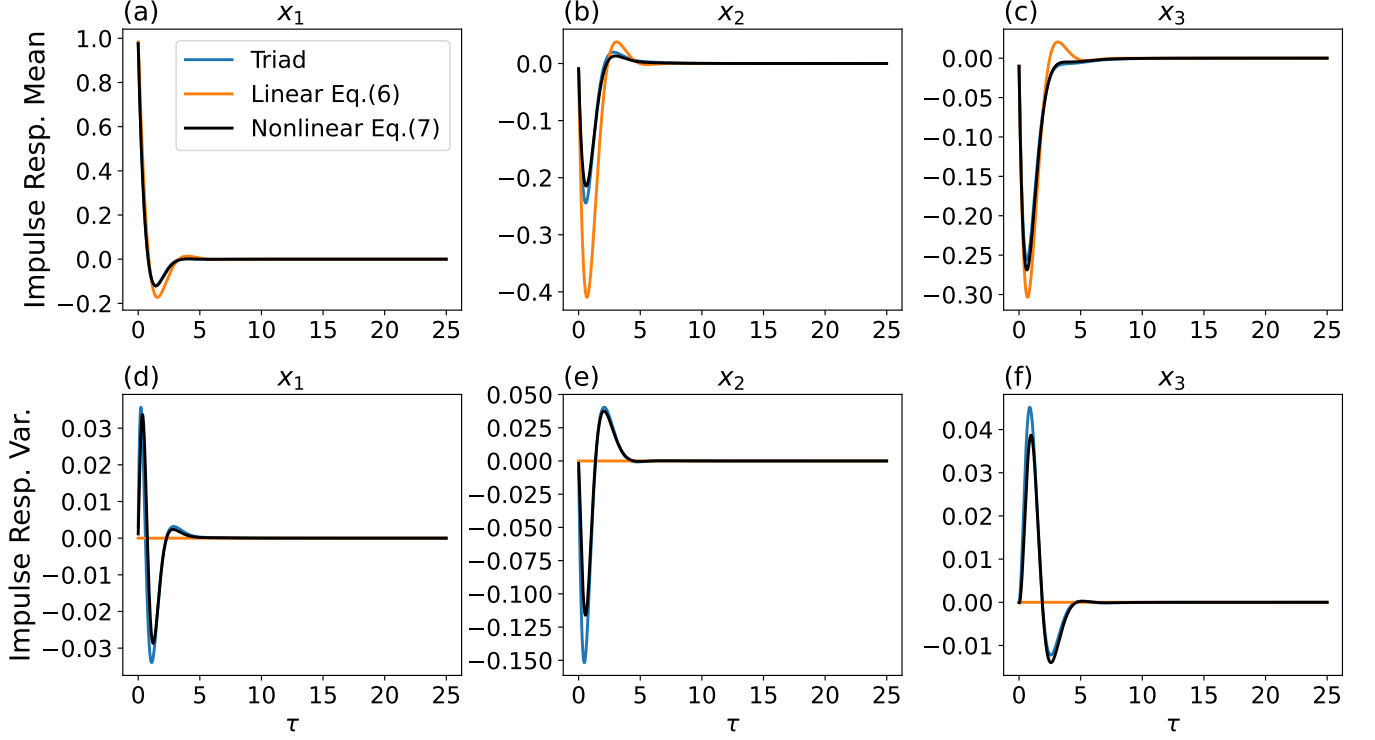


FIG. 2. Impulse response functions as modeled by the original triad system in Eq. (5), the linear emulator in Eq. (6) and the neural emulator in Eq. (7). First row: response of the ensemble mean to *impulse* perturbations imposed on  $x_1(0)$  at time  $t = 0$ . Second row: response of the ensemble variance to *impulse* perturbations imposed on  $x_1(0)$  at time  $t = 0$ . Impulse response functions are computed using an ensemble size of  $N_e = 10^5$  members.

*b. Responses to a specific logarithmic forcing.* Having evaluated the ability of the data-driven neural model to capture the impulse response operator, we now consider a more targeted test involving a specific, time-dependent forcing. We introduce a logarithmic forcing term to the right-hand side of the original triad model (Equation (5)), the linear model (Equation (6)), and the neural model (Equation (7)). The forcing is applied only to the first mode

$x_1$  and takes the form  $(0.01\log(1+t), 0, 0)$  per time step. Each model is integrated for 2500 time steps (25 Model Time Units), and we compute the difference between the forced and unforced simulations in terms of ensemble-mean and ensemble-variance responses. Results are presented in Figure 3. The neural model accurately reproduces the forced responses across all three components. The linear model performs qualitatively well but exhibits significant deviations in the ensemble-mean response of the second mode  $x_2$  as shown in Figure 3(b). This is consistent with the earlier Section: the largest error in the linear model’s impulse response also occurred in  $x_2$  (see Figure 2(b)). This supports the interpretation that accurately capturing the impulse response operator is critical for a model’s reliability in predicting responses to general, time-dependent forcings. As expected from the analysis of the response operator, the linear model is not able to capture the response in ensemble variance. The neural model shows skillful response, capturing the time-dependent changes in ensemble variance relatively well, with the largest error in the second mode  $x_2$ . In general, considering that the changes in variance are very small, we conclude that the neural emulator is skillful in responding to the imposed logarithmic forcing.

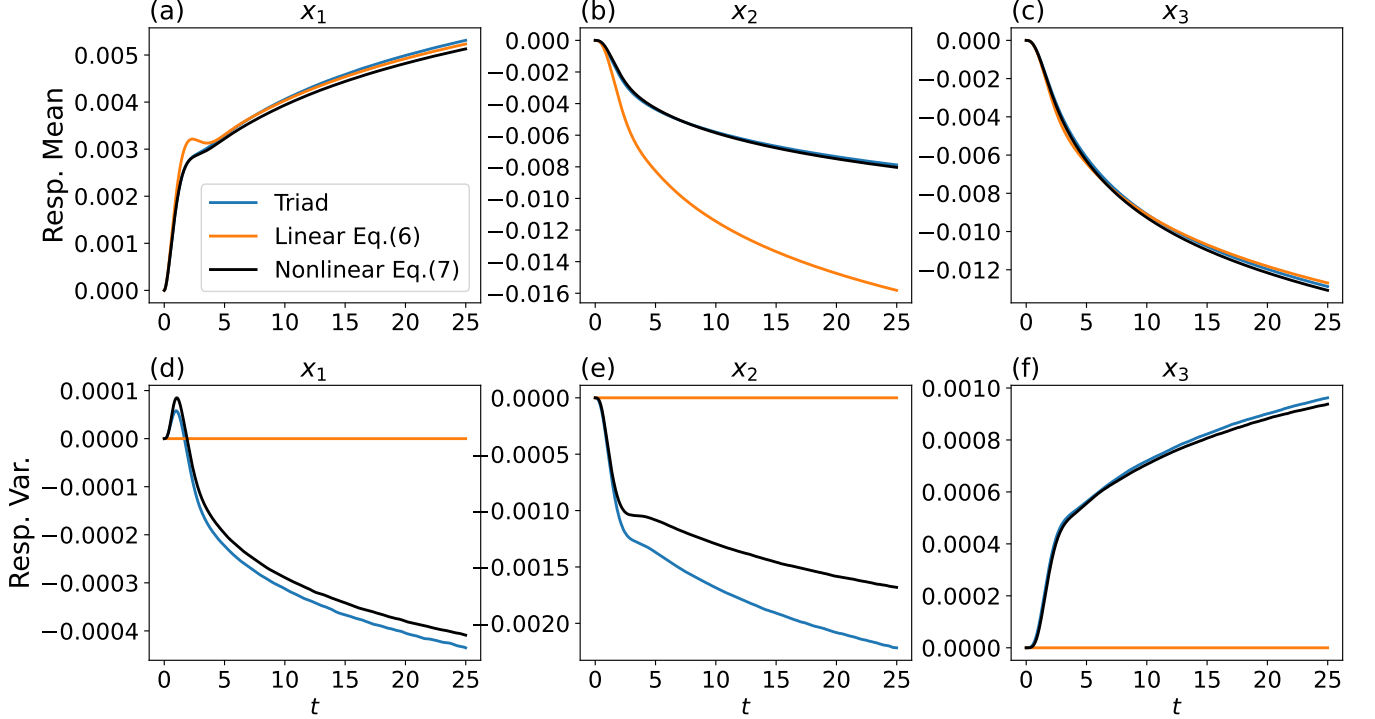


FIG. 3. Response to a small logarithmic forcing  $F = (0.01\log(1+t), 0, 0)$  imposed on the right-hand-side in Eq. (5), the linear emulator in Eq. (6) and the neural emulator in Eq. (7). First row: response of the ensemble mean to external forcing. Second row: response of the ensemble variance to external forcing. Responses are computed using an ensemble of  $N_e = 10^5$  members.

#### 4. Main takeaways

Given a (practically) infinitely long trajectory of a stochastic dynamical system, and assuming the ideal condition where the full state vector is observed, it is possible to construct a neural stochastic model that is stable, reproduces the stationary statistics, and responds accurately to small but general external perturbations and forcings. While these results are encouraging, they remain far from any real-world scenario. In practice, even when a low-dimensional *effective* dynamics exists, the main challenge is that we typically have access only to partial observations of a complex, interconnected system. Such challenges lead to the important problem of having to choose the *proper* variables to model as well as the proposal of stochastic parametrizations to account for the unobserved degrees of freedom.

### C. Data-driven modeling when we do not observe the full state vector

We now return to the triad model defined in Eq. (5) and consider the more realistic scenario of model inference under partial observations and multiple timescales. The parameters chosen for this test are:  $L_{11} = -2$ ,  $L_{12} = 0.2$ ,  $L_{13} = 0.1$ ,  $\gamma_2 = 0.6$ ,  $\gamma_3 = 0.4$ ,  $\sigma_2 = 1.2$ ,  $\sigma_3 = 0.8$ ,  $I = 1$ ,  $\epsilon = 0.01$ . In this setting the variable  $x_1$  clearly is the slow mode, forcing the much faster modes  $x_2$  and  $x_3$ . We again integrate the system in (5) with an Euler–Maruyama scheme for a period of length  $T = 10^7$  with time step  $dt = 0.01$  (i.e.  $10^5$  Model Time Units).

Unlike the case considered in the previous section, where the entire state vector  $\mathbf{x}(t) = [x_1, x_2, x_3](t)$  was available, we now consider a more challenging scenario: only one component of the system is observed (or available or chosen), either  $x_1$ ,  $x_2$ , or  $x_3$ . The modeling task is thus reduced to constructing a scalar stochastic model for the observed component alone. We require the scalar stochastic model to satisfy two criteria:

- i. it must reproduce the statistics of the observed component;
- ii. it must correctly captures its response to perturbations as in the original triad system.

Criterion (ii) is particularly demanding because, in the triad system defined by Eq. (5), perturbations can propagate through the network of interacting variables, inducing cascades of feedbacks. These time-dependent feedback loops must be effectively parametrized within the scalar model, despite the absence of direct observations of some components. While clearly nontrivial, this problem is representative of real-world data-driven modeling scenarios, where models are often built from partial observations of high-dimensional systems.

Proposing a scalar data-driven model from partial observations that satisfies the two criteria above raises two central challenges:

- *Choice of variable to model.* The derived reduced order model is now dependent on the variable we choose to model. Not all components can be modeled to meet the above criteria. In the simple case considered here the choice of  $x_2$  or  $x_3$  will be wrong as these two modes represent the fast dynamics forced by the much slower mode  $x_1$ . Therefore, it would be impossible to parametrize the effect of  $x_1$  from information of  $x_2$  or  $x_3$  alone. The only possible way forward is to choose the slow mode  $x_1$ . Identifying such a *proper* variable is a necessary prerequisite for constructing a meaningful model in the presence of only partial observations [31, 37, 52, 69].
- *The need for suitable parametrizations.* Having identified the proper variable  $x_1$  to model, the next challenge is to appropriately parametrize the cumulative effects of the unresolved components  $x_2$  or  $x_3$  onto the slow mode  $x_1$ . This leads to the classic problem of stochastic parametrization [1, 2, 39, 100–102]. As we will show, the success of the resulting model, particularly in capturing forced responses, hinges critically on the quality of this parametrization.

#### 1. Functional form of the reduced order models considered

Given the correct choice of variable  $x_1$  to model we can now proceed in proposing the two data-driven scalar models considered. As in the previous Section, to keep the main text focused and readable, we leave the technical details of the fitting procedures for Appendix A. We consider two nonlinear, neural models differing with the stochastic parametrization considered:

- *Neural model with additive noise.* We consider the following neural model fitted using an artificial neural network, i.e. a Multilayer Perceptron (MLP) with one hidden layer. The model takes the following form:

$$dx = (Lx + n(x))dt + \sigma dW, \quad (8)$$

$L$  is a linear operator (here just a scalar),  $n(x)$  is a nonlinear operator and  $\sigma^2$  is the noise variance.  $W$  is the standard Wiener process. Note: the whole drift  $(Lx + n(x))$  is fitted by the neural network.

- *Neural model with multiplicative noise.* We consider a neural model as before, but now defined with multiplicative rather than additive noise:

$$dx = (Lx + n(x))dt + \sigma(x)dW. \quad (9)$$

Differently from the previous model in Eq. (8), now the noise is also state dependent. The multiplicative noise  $\sigma(x)$  is fitted with an additional neural network, see Appendix A. As before, we are going to often refer to the two models above as “neural model” or “neural emulator”.

To train the two models above we consider a long simulation of the triad system in Eq. (5) using the set of parameters reported in Section III C. We then extract only the time series of  $x_1$ . The two models in Eq. (8) and (9) are then trained on this long, scalar time series of  $x_1(t)$  alone.

## 2. Stationary and perturbed statistics of the scalar model

We integrate the two data-driven scalar models and specified in Eq. (8) and (9) for  $T = 10^7$  time steps, yielding time series of the same length as the time series of  $x_1(t)$  obtained from the long integration of the triad system used for training. To evaluate the models' ability to capture both stationary and perturbed statistics, we examine the stationary probability distribution and the impulse response functions. Specifically, we focus on responses in the ensemble mean and variance by studying the time dependent change of the perturbed probability distribution  $P_p(x, t)$  (where the subscript “ $p$ ” stands for “perturbed”) to impulse perturbations in the variable  $x$  itself, see Section II B for more details.

The neural model with additive noise (Figure 4(a)) fails to accurately capture the stationary statistics in a quantitative way. Moreover, the ensemble mean response to an impulse perturbation decays too slowly, and notably, the model fails to reproduce any significant response in the ensemble variance. In contrast, incorporating multiplicative noise (Eq. (9)) leads to a substantially improved representation of the stationary distribution, as seen in Figure 4(e), which closely matches the true distribution. The mean response remains largely unchanged, decaying too slowly, but the model now captures a qualitatively correct signal in the ensemble variance, albeit with a similarly slow decay.

These results indicate that the inclusion of multiplicative noise improves the reduced-order model's ability to represent both stationary statistics and variance responses to perturbations. In the full triad system, a perturbation to  $x_1$  at time  $t = 0$  leads to changes in  $x_1$ ,  $x_2$  and  $x_3$  at the next time step  $dt$ . Consequently,  $x_2$  and  $x_3$  feedback on  $x_1$  at the consequent time step. This leads to a cascade of state-dependent interactions until the system relaxes back to stationarity. Such complex, state-dependent feedbacks cannot be represented by additive noise alone and require the inclusion of state dependent noise  $\sigma(x)$ , effectively parametrizing such interactions. However, even when multiplicative noise is considered, the responses to impulse perturbations are still only qualitatively right. The example illustrates that accurately capturing stationary statistics does not guarantee faithful reproduction of perturbed statistics.

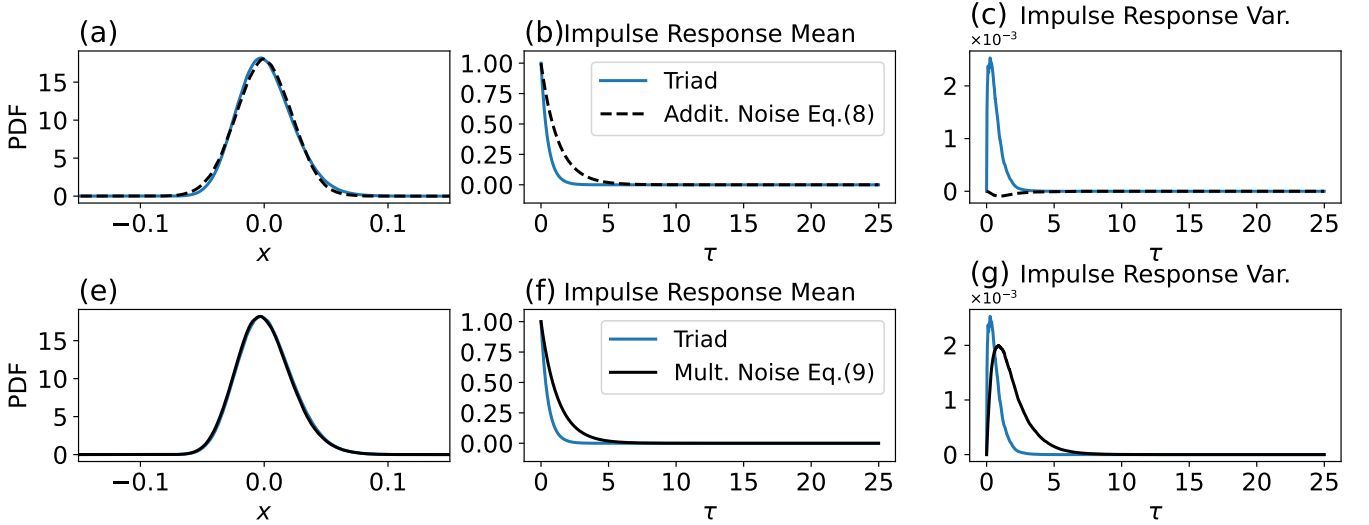


FIG. 4. First row: stationary probability distribution (panel (a)); ensemble mean response to an impulse perturbation (panel (b)); ensemble variance response to an impulse perturbation (panel (c)) for the variable  $x_1$  in the triad system in Eq. (5) and the variable  $x$  in the neural scalar emulator with additive noise in Eq. (8). Second row: same as the first row but we are now considering the neural scalar emulator with multiplicative noise in Eq. (9). Impulse response functions are computed using an ensemble of  $N_e = 10^5$  members.

The presence of slowly decaying responses in the ensemble mean and variance to perturbations is indicative of a system that is no longer Markovian. The reduced-order stochastic scalar model is trained solely on the time series of  $x_1(t)$ . However, the time series  $x_1(t)$  is generated by the full triad system in Eq. (5) and implicitly reflects the

influence of the unobserved variables  $x_2$  and  $x_3$  on it. The variability of the unobserved variables  $x_2$  and  $x_3$  manifest as memory effects in the reduced order scalar model for  $x_1$ . One strategy for addressing such memory effects is the multilevel regression approach first introduced by Kratsov, Kondrashov and Ghil (2005) [6] and later generalized by Kondrashov, Checkroun and Ghil (2014) [7]. The multilevel regression strategy method augments the reduced-order model with a hierarchy of linear equations solving for the residuals from the deterministic dynamics, and can be thought as a practical implementation of the Mori–Zwanzig formalism in statistical mechanics [2, 7]. Ultimately, the remaining residuals become white in time, allowing the system to be closed using a Wiener process. Similarly, it could be possible to address the issue through recurrent neural networks [103]. An alternative, practical approach for handling non-Markovian effects is to coarse-grain the data in the temporal dimension, for instance, by averaging over a time window. This suppresses fast fluctuations within that window leading to an effective “Markovianization” of the the dynamics. Due to its simplicity and ease of implementation, this method is commonly used in the literature (see for example [4]) and is also adopted in the present study.

We therefore consider again the time series  $x_1(t)$  from the long simulation of the triad system in Eq. (5). As an additional step, we average the time series over a short temporal window of 10 time steps (recall that  $dt = 0.01$ , so this is equivalent to 0.1 Model Time Units). Importantly, this is not equivalent to sub-sampling the original dynamics by taking every 10th data point. Instead, averaging over a 10-step window smooths out fast variability and effectively defines a new, coarse-grained “more Markovian” system. We then re-train the neural models with additive and multiplicative noise on the new coarse-grained data. Next, we simulate the neural models over long timescales to analyze their stationary distributions, as well as their ensemble mean and variance responses to impulse perturbations. Results are shown in Figure 5. As before, the stochastic model with additive noise fails to capture the correct stationary statistics (Figure 5(a)). While the response in the ensemble mean improves relative to the non-coarse-grained case, the response in ensemble variance remains suppressed. In contrast, the model with multiplicative noise not only captures the stationary distribution and further improves the mean response, but now also closely reproduces the response in variance, capturing the peak magnitude and deviating only slightly in its temporal decay. Note that the stationary response in ensemble mean and variance to impulse perturbations of the original degree of freedom  $x_1$  are the same in both Figures 4 and 5, the only thing changing in the latter is that the reduced-order model is defined in a coarse-grained dynamics.

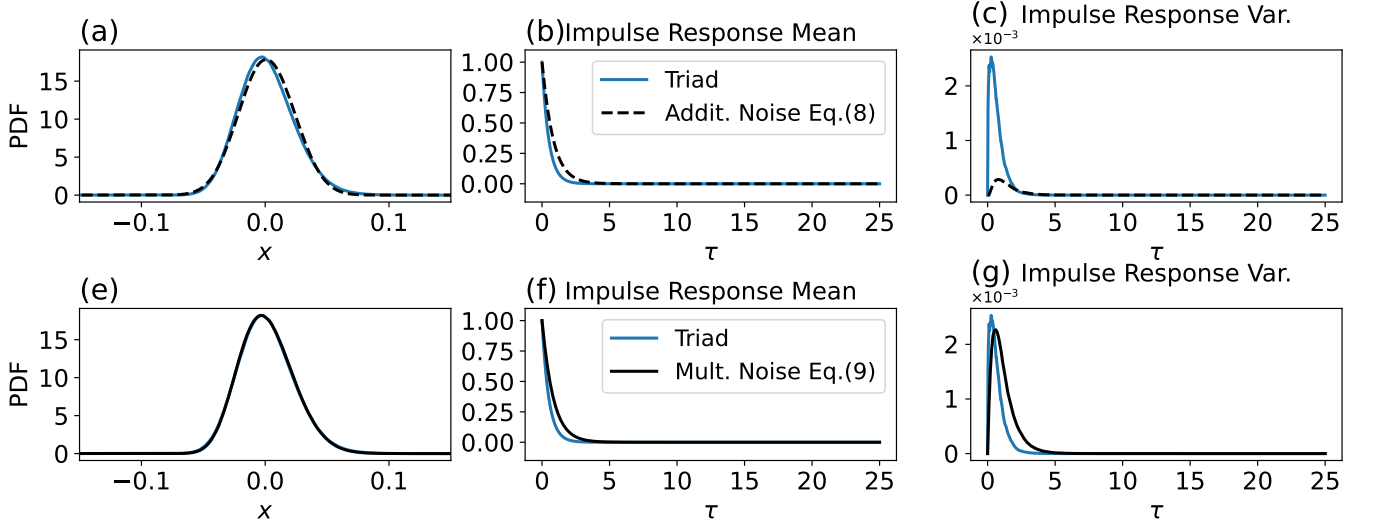


FIG. 5. Same as in Figure 4 however here the scalar emulators in Eq. (8) and Eq. (9) have been trained on a long trajectory of  $x_1(t)$  after coarse-graining by averaging every 10 time-steps. No additional preprocessing was performed for the original triad system in Eq. (5), i.e. the blue curves in this Figure and in Figure (4) are the same.

### 3. Main takeaways

Even with access to very long time series, modeling real-world dynamical systems from data alone remains fundamentally constrained by observing only a subset of the full state vector. This leads to two major challenges: (i)

the resulting data-driven model will depend heavily on the specific variable chosen for modeling, and (ii) once a suitable slow variable is identified, the cumulative effect of the unobserved degrees of freedom must be appropriately parametrized. These issues, demonstrated at the “practical level” within the context of a low-dimensional model, become even more severe in realistic high-dimensional systems, which often lack a clear time-scale separation. These challenges are intrinsic to data-driven approaches for dynamical systems, and simply extending time series length or training increasingly large neural networks is unlikely to resolve them.

The core difficulty is conceptual: there is no rigorous mathematical framework for selecting the *proper* variables to model in real-world, high-dimensional dynamical systems. This poses fundamental limitations for purely data-driven approaches. In practice, such choices rely on physical intuition and prior knowledge. When possible, selecting the right variables amounts to identifying an appropriate coarse-grained description of the dynamics, including relevant fields and suitable spatial and temporal scales. Consequently, effective data-driven modeling of real-world complex systems hinges on deep physical insight and strong domain expertise.

#### IV. A REAL-WORLD EXAMPLE: RADIATIVE RESPONSES TO TEMPERATURE PERTURBATIONS IN A CLIMATE MODEL

Building on the ideas discussed above, we present a stochastic reduced-order model tailored to a real-world application. The emulator is designed to capture the large-scale dynamics of sea surface temperature (SST) and the global mean net radiative flux at the top of the atmosphere (TOA). To achieve this, we restrict our focus to a limited range of spatiotemporal scales by selecting a few dominant modes, using monthly-averaged data, and high-pass filtering to remove multidecadal variability. The cumulative impact of fast, unresolved processes on the slow dynamics is parametrized by multiplicative, state-dependent noise. We then evaluate the model’s response to temperature changes and assess its utility in improving our understanding of radiative feedbacks.

##### A. Scientific problem at hand

Radiative forcing (e.g., as resulting from a change in  $\text{CO}_2$  concentration) drives warming in the Earth system, leading to changes in sea surface temperatures (SSTs) and associated radiative feedbacks. Recent studies have shown that even given the same global mean temperature warming, different spatial patterns of SST warming can produce markedly different radiative feedbacks. For example, warming concentrated in the eastern Pacific tends to produce positive radiative feedbacks, thereby amplifying the initial temperature change. In contrast, greater warming in the western Pacific or warm-pool region tends to have a stabilizing effect [29, 30]. This sensitivity of the Earth’s energy imbalance to the spatial pattern of surface temperature change is commonly referred to as the “pattern effect”. The pattern effect captures the fast response of top-of-atmosphere (TOA) radiative fluxes to spatial variations in temperature. It is theoretically defined in the framework of energy balance models by Taylor expanding the radiative response over the steady state temperature (see for example Section 2 of Meyssignac et al. (2023) [104]). A general data-driven framework to explore radiative responses from data has recently been proposed in [105], with the pattern effect arising as a limiting case in the case of fast responses. The framework in [105] focuses on both *direct* causal links between SST and radiative fluxes as well as *cumulative* (in time) links.

A widely used approach to study the relationship between SST patterns and TOA radiative fluxes is through Green’s function experiments [106], in which the radiative response to localized SST perturbations is quantified using atmosphere-only models [30, 107–110]. These experiments are extremely valuable for rigorously testing model sensitivities. However, they are computationally expensive and typically require large SST perturbations (e.g., 1–4 K) to generate a measurable response within short simulations. These large perturbations can lead to nonlinear responses, invalidating the linearity assumptions adopted in the Green’s function framework [111]. There is therefore a need for fast and interpretable data-driven models capable of performing large-ensemble experiments at low computational cost and with small perturbation amplitudes. Moreover, climate models are known to be biased, while data-driven emulators offer, in principle, a way to learn climate dynamics directly from observations.

There are two broad strategies to build such emulators. One is to construct a general-purpose emulator of the entire climate system and then use it to study specific problems. However, as shown by Van Loon et al. (2025) in the context of the ACE2 emulator [28], this strategy may not always succeed. A second, more traditional and targeted approach is to design an emulator focused on the problem at hand, e.g. [5]. While this approach sacrifices generality, it offers important advantages: the focus on a specific problem often comes together with a greater understanding of

what are the proper variables to model as well as the spatial and temporal scales to consider. These choices, typically informed by physical intuition and prior literature, can directly shape the architecture and inputs of the emulator. Moreover, by isolating only core relevant processes for the specific problem considered, such an emulator can remain interpretable, thereby helping to bridge the gap between simulation and understanding [55].

### B. A reduced order model of surface temperature and radiative fluxes

Given the general problem outlined above, we aim to build a skillful emulator of sea surface temperature and radiative fluxes that allows us to study stationary and perturbed statistics. Building on the previous Sections we consider a functional form of the neural model defined follows:

$$d\mathbf{x} = (\mathbf{L}\mathbf{x} + \mathbf{n}(\mathbf{x}))dt + \mathbf{\Sigma}(\mathbf{x})d\mathbf{W}, \quad (10)$$

Where  $\mathbf{W}$  is the standard Wiener process. As in the previous Sections, we use a neural network to fit the drift part  $(\mathbf{L} + \mathbf{n}(\mathbf{x}))$  and another network to fit the multiplicative noise  $\mathbf{\Sigma}(\mathbf{x})$ . As before, to improve readability we refer to Appendix A for technical details.

We now face the challenging task of selecting appropriate preprocessing steps to define the coarse-grained dynamics to be modeled. These coarse-graining choices are crucial, as the real climate system involves not only SST and radiative fluxes, but also many other interacting variables, i.e. this is a practical example of the case of a partially observed state vector. We now describe the dataset used for this experiment, along with the preprocessing steps taken. The preprocessing procedure largely follows that described in [105] and we will refer the reader to that work for additional details and clarifications where needed.

#### 1. Data, preprocessing and coarse-graining

*a. Data.* The focus is on a state-of-the-art coupled climate model GFDL-CM4 [112]. The model offers data from a long control run simulating the coupled climate system for 600 years with constant  $\text{CO}_2$  fixed at pre-industrial level. The ocean component is the MOM6 ocean model [113] with a horizontal grid spacing of  $0.25^\circ$  and 75 vertical layers. The atmospheric component is the AM4 model [114, 115] with a horizontal grid spacing of roughly 100 km and 33 vertical layers. The model considered in Eq. (10) will be trained on the long control run. The variables considered are two: SST and the global mean net radiative flux at the top of the atmosphere (hereafter, often referred to as TOA). The focus on global mean net radiative flux, rather than its spatiotemporal representation is motivated by the fact that such variable does not show large scale patterns of variability. It is in fact a fast variable in respect to SST and the main signal we are interested in is its global average. The SST field is considered only in the latitudinal range  $[-45, 45]$ , a choice informed by earlier studies highlighting the prominence of radiative feedbacks in the tropics and subtropics [30, 108].

*b. Preprocessing and coarse-graining.* Climate dynamics is not only encompassing the SST and radiative fluxes. Therefore, we aim in building a reduced order model focusing on the slow dynamics and parametrizing unobserved degrees of freedom as noise. We consider the control run and proceed in coarse-graining both the spatial and temporal scales. First, starting from daily data, we compute monthly averages. We then remove the seasonal cycle from both the SST and radiative fluxes, allowing us to focus on seasonal anomalies, rather than periodic signals driven by the annual solar forcing. We then decompose the SST spatiotemporal field in a set of  $n$  modes, i.e. empirical orthogonal functions (EOFs). Projecting the computed EOFs onto the original data give us  $n$  Principal Components (PCs). In formulae, given the SST field  $\mathbf{X}(t) \in \mathbb{R}^N$ , we decompose it as:

$$\mathbf{X}(t) = \sum_{i=1}^n x_i(t)\mathbf{e}_i + \sum_{j=n+1}^N y_j(t)\mathbf{e}_j, \quad (11)$$

and retain only the first  $n = 20$  modes  $x_i(t)$ , while the remaining components  $y_j(t)$  represent the fast modes.  $\mathbf{e}$  are orthonormal bases (i.e. the EOFs). Therefore, the time series  $x_i(t)$  will be used to train the emulator in Eq. (10). These two steps, i.e. one month averaging and the projection over EOFs, attempt to define a new coarse-grained system for the slow variability of the SST field. Note that Penland and Sardeshmukh [4] and Penland (2006) [5] already showed how a similar preprocessing would lead to a skillful linear Markov model of the tropical Pacific SST. These SST principal components are then concatenated with the scalar net radiative flux time series: to simplify the

notation, we are going to refer to the state vector of the reduced order model as simply as  $\mathbf{x}(t) \in \mathbb{R}^{n+1}$ .

Is a 600 year-long control run a long-enough simulation to learn a model of SST and radiative fluxes? Whether this is a sufficiently long simulation depend on whether the time series considered sample enough recurrences, see Cecconi et al. (2012) [31]. In a multiscale system like climate, even in the presence of constant external forcing, we observe processes such as multidecadal oscillations which are only sampled a few times in a 600-year long experiment. Therefore, we make the following choice: we high-pass filter the data with a cut-off frequency of  $10^{-1}$  years. This removes all low-frequency variability which we would have little chance to learn from data in the first place, and focus on variability inside 10 years only. This choice involves a trade-off: our model will not be able to capture multidecadal variability and we will restrict ourselves to explore subdecadal variability only. At the same time this leads to an effectively larger sample size than we would have had by keeping all time scales. Additionally, this step also allow us to remove drifts present in the control run of the CM4 run, mainly coming from an ocean component that still did not equilibrate.

In this paper we will focus on testing the ability to “generalize” to unseen climate scenarios: we will fix the SST variable with a precomputed trajectory coming from two, 150 years long forced runs, namely a 1pctCO<sub>2</sub> and 4×CO<sub>2</sub>, and use this information to reconstruct the change in global mean TOA in these simulations. The 1pctCO<sub>2</sub> is an idealized experiment simulating the climate system under a 1% CO<sub>2</sub> increase per year starting from pre-industrial conditions. The 4×CO<sub>2</sub> is an idealized experiment simulating the climate system under an abrupt quadrupling of CO<sub>2</sub> concentration from its pre-industrial level at time  $t = 0$ . Importantly, considering the 1pctCO<sub>2</sub> and 4×CO<sub>2</sub> simulations leads to an additional challenge: the radiative fluxes are directly influenced by an increase in atmospheric CO<sub>2</sub>. However, our reduced order model only has access to SST and radiative fluxes and it cannot explicitly include CO<sub>2</sub> concentration. To address this, we remove the portion of the net TOA radiative flux that is attributable solely to rising CO<sub>2</sub>. This allow us to isolate and study the component of radiative feedback that is driven by changes in SST. This correction relies on the well established fact that the global-mean radiative forcing from CO<sub>2</sub> alone increases approximately logarithmically with its concentration [116, 117]. As is standard, for the 4×CO<sub>2</sub> experiment, we remove a standard constant of  $8Wm^{-2}$  [118]. For the 1pctCO<sub>2</sub> run we instead apply a time-dependent correction of the form  $\alpha \log[C_t/C_0]$ ;  $C_0$  and  $C_t$  respectively representing the concentration of CO<sub>2</sub> in the control run and forced experiments.

We note that considering 1 month averages in TOA fluxes is not arbitrary: the immediate response of TOA fluxes to perturbations in SST is fast (e.g.,  $\sim 20$  days in tropical large-scale convective overturning motion in the GFDL-CM4 model). Therefore, reconstructing the net radiative fluxes given information of the SST in the two forced runs above is a relatively easy task for this system and it converts to a 1 time step prediction. For this point we refer the reader to the conceptual discussion in Section 7 of [105]. In other words, the preprocessing considered here maximizes the chance of having a data-driven model that correctly reconstruct the TOA variable in unseen climates.

## 2. Stationary statistics and forced responses

*Stationary statistics.* Given the  $n + 1$  state vector  $\mathbf{x}(t) \in \mathbb{R}^{n+1}$  defined in the preprocessing step above, we can now train the emulator defined in Eq. (10) on the long control run of the GFDL-CM4 model. The trained emulator is then used to simulate a 600 years long climate trajectory (same length as the one used in the original model GFDL-CM4). The stationary probability distributions of the first SST mode and of the net radiative flux at the TOA are found to be qualitatively well captured, see Figure 6(a,b). The largest discrepancies between the emulator and the original model are found for the autocorrelation functions. Autocorrelation functions are shown for the first SST mode (largely corresponding to the El Niño Southern Oscillation (ENSO) [119]) and for the TOA variable.

*Forced responses.* The pattern effect problem discussed in IV A concerns identifying a direct causal link between patterns of SST warming and changes in radiative fluxes at the TOA. Before attempting any mechanistic interpretation or physical understanding, we first assess whether the neural model we have built possesses predictive skill in capturing forced responses. Specifically, we test if the neural model can be used to reconstruct the global mean radiative flux from a pre-computed, forced sea surface temperature field in forced experiments. In doing so, we also test an important question in neural models: is the neural network model able to generalize to out-of-distribution predictions? To answer these question we consider the two, 150-years long, forced runs of the GFDL-CM4 climate model introduced in Section IV B 1. We extract the sea surface temperature from these forced runs and project it onto the set of  $n = 20$  EOF bases found in the control run. We refer to such forced modes as  $\mathbf{x}_{\text{SST}}^f$ . We then simulate the neural emulator for 150 years by constraining the SST degrees of freedom to be exactly equal to  $\mathbf{x}_{\text{SST}}^f$ . Given  $\mathbf{x}_{\text{SST}}^f(t)$  the model returns the TOA variable,  $x_{\text{TOA}}(t + 1)$ , at the next time step, starting from initial condition  $x_{\text{TOA}}(0) = 0$ . The results is shown in Figure 6(e,f). In both the case of 1pctCO<sub>2</sub> or 4×CO<sub>2</sub> runs, the model is able to reconstruct the change



in radiative fluxes at the TOA in a quantitative way. We highlight that our preprocessing allowed us to reduce this reconstruction step into a prediction of the 21-st entry of the state vector at time  $t + 1$ , given information of the first 20 entries at the previous time  $t$ . This is only possible because of our focus on 1-month averages: the radiative fluxes at the TOA largely respond already at a sub-monthly time scales to temperature perturbations, therefore allowing us to focus on a direct statistical link  $\mathbf{x}_{\text{SST}}(t) \rightarrow x_{\text{TOA}}(t + 1)$ . We also note that it is perhaps surprising that the neural network is able to respond faithfully even when for nonstationary inputs and with temperature values far out of the training distribution (in physical units, the mean temperature anomaly shifts from a  $0K$  to  $5K$  from the control in both forced simulations).

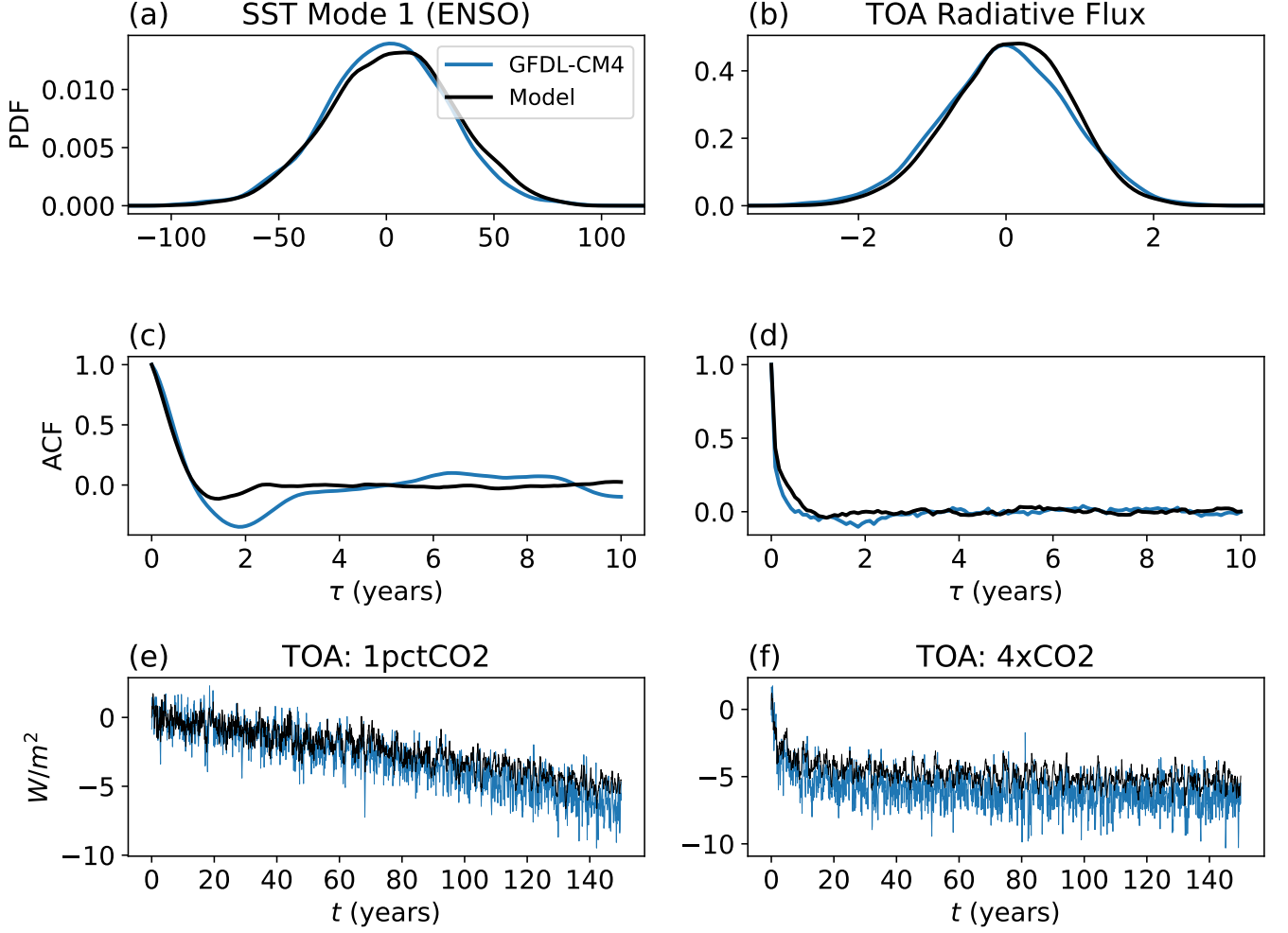


FIG. 6. Panel (a): stationary distributions obtained for the 1st principal component of the sea surface temperature (SST) field as in the original GFDL-CM4 climate model and as emulated by the neural emulator with multiplicative noise in Eq. (10). Units: nondimensional. Panel (b): same as panel (a) but for the global mean radiative flux at the top of the atmosphere (TOA). Units:  $W/m^2$ . The stationary distributions have been obtained after simulating the neural emulator for 600 years. Second row: same as the first row but for the autocorrelation functions. Third row: reconstruction of the net radiative flux at the TOA by the neural emulator in Eq. (10) after constraining the SST degrees of freedom to follow a precomputed trajectory in two forced experiments in the GFDL-CM4 model. The forced experiments considered are the 1pctCO<sub>2</sub> and 4xCO<sub>2</sub>, see Section IV B 1 for details. Note: the net flux at the TOA variable is negative upward (i.e., leaving the planet).

### 3. Interpretability and understanding

In the previous Section we showed that the neural emulator proposed in this study can in fact be used to reconstruct the instantaneous change in radiative feedback at the top of the atmosphere given pre-computed changes in the temperature field. As emphasized before, the task of the emulator in the reconstruction/prediction task reduces to the following mapping:  $\mathbf{x}_{\text{SST}}^f(t) \rightarrow x_{\text{TOA}}(t+1)$ , where  $\mathbf{x}_{\text{SST}}^f(t) \in \mathbb{R}^n$ ,  $x_{\text{TOA}}(t) \in \mathbb{R}$  and with initial condition  $x_{\text{TOA}}(0) = 0$ . We now ask the following question: *What are the SST patterns that contribute the most to this skillful prediction?* To answer this question, we must go beyond the prediction task presented above and identify which components of the sea surface temperature input contributes the most to changes in radiative flux. We explore this question through the framework of linear response theory, by capturing the *direct* causal link  $x_{j,\text{SST}}(t) \rightarrow x_{\text{TOA}}(t+1)$ , where  $x_{j,\text{SST}}(t)$  represents the  $j$ -th component of the surface temperature field at time  $t$ .

We briefly describe the strategy to infer this direct causal link with response theory, and refers to Section II B for details. We consider the neural emulator in Eq. (10) and iteratively perturb the  $j$ -th sea surface temperature component of the state vector at time  $t = 0$  with a small *impulse* perturbation  $x_j(0) + \Delta_j \delta(t)$ .  $\delta(t)$  being a Dirac delta and  $\Delta_j$  being a perturbation of very small amplitude. The amplitude  $\Delta_j$  depends on the component  $x_{j,\text{SST}}$  itself (Section II B). We then compute the ensemble mean response of the net radiative flux at the TOA at the next time step  $t = 1$ , referred here as  $\delta\langle x_{\text{TOA}}(1) \rangle$ . To estimate the ensemble mean response we consider  $10^3$  initial conditions. We write this response as follows:

$$R_{\text{TOA},j}(1) = \frac{\delta\langle x_{\text{TOA}}(1) \rangle}{\Delta_j \delta(t)}, \quad (12)$$

ad remind the reader that the index  $j$  only considers the SST degrees of freedom. Therefore, the response at 1-time-step  $R_{\text{TOA},j}(1)$  defines the direct causal link  $x_{j,\text{SST}}(t) \rightarrow x_{\text{TOA}}(t+1)$  between the  $j$ -th degree of freedom in SST and the net radiative flux at the TOA.

The vector  $\mathbf{R}_{\text{TOA}}(1) \in \mathbb{R}^n$  is projected back to the higher, original  $N$ -dimensional space. To do so we consider the previously computed EOFs, i.e. the orthonormal vectors  $\mathbf{e} \in \mathbb{R}^{n,N}$  and project the 1-time-step responses as follows:

$$\mathbf{S} = \mathbf{R}_{\text{TOA}}(1) \cdot \mathbf{e} = \sum_j^n R_{\text{TOA},j}(1) \mathbf{e}_j, \quad (13)$$

where  $\mathbf{S} \in \mathbb{R}^N$  is a sensitivity map defined in the high-dimensional  $N$  dimensional space. Such map approximates at each grid point  $i$  in the ocean, the sensitivity  $\frac{\partial x_{\text{TOA}}}{\partial x_{\text{SST},i}}$ , where  $x_{\text{TOA}}$  is the global mean radiative flux at the TOA and  $x_{\text{SST},i}$  is the SST at grid point  $i$ .

The sensitivity map  $\mathbf{S}$  obtained using the neural emulator in Eq. (10) is shown in Figure 7. The obtained sensitivity map is in qualitative agreement with previous results in response theory (Figure 2(a) in [105]), with other data-driven approaches (see for example Figure 7(b) in [120] and Figure 2 in [121]), but, most importantly, with the sensitivity map obtained by directly perturbing the SST boundary condition of atmosphere-only climate models (see third row of Figure 2 in [29], see Figure 5(a) in [30]). Note that in the latter case, the maps exhibit fewer spatial features due to the coarse resolution of the perturbation patches, which span tens of degrees. The marked feature of this sensitivity map is the sensitivity dipole found the tropical Pacific, with negative values on the western side of the basin and positive values on the eastern side, see for example [30]. This means that an initial warming in the eastern Pacific basin will result in a direct, positive radiative feedback, further amplifying the imposed temperature change; the opposite is true for the western Pacific. The mechanistic explanations for such mechanisms can be found for example in [111, 122] and we refer the interested reader to these papers for details. In brief, the positive sensitivity in  $\mathbf{S}$  in the eastern Pacific is associated with a high-climatology of low-level clouds: a warming perturbation is expected to decrease the cloud cover, leading to anomalies in incoming shortwave radiation and therefore a positive sensitivity. On the other hand, the western Pacific is a region dominated by deep convective phenomena. Because of this, a surface temperature warming in the western Pacific basin tend to travel vertically through the troposphere and then horizontally through gravity waves. This process strengthen the inversion layer in the eastern Pacific basin (and in other regions with high-climatology of low-level clouds), leading to a larger low-level cloud fraction and increasing the reflected shortwave at the top of the atmosphere.

To conclude this Section, the analysis in Figure 7 confirms that the good reconstruction observed in the forced regime (Figure 6(e,f)) arises for the physically correct reasons.

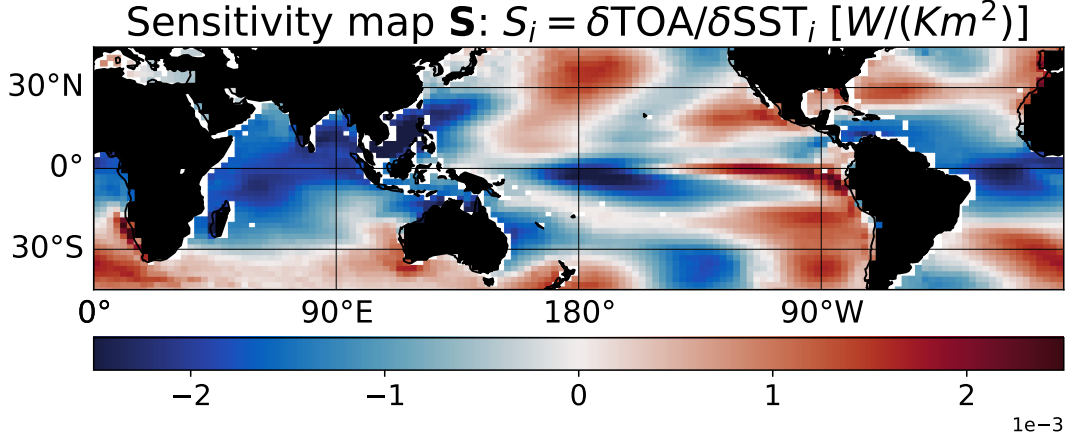


FIG. 7. Sensitivity map obtained using the neural emulator in Eq. (10). At each grid point  $i$  we are plotting the 1 time step response in the global mean, net radiative flux at the top of the atmosphere (TOA) driven by an impulse perturbation in the sea surface temperature (SST) at that grid point. Note: the computation is done in a 21 dimensional space spanned by a set of empirical orthogonal functions and this map is a projection of the results obtained in the low-dimensional space. The response has been obtained by averaging over an ensemble of  $10^3$  initial conditions.

#### 4. Main takeaways

In this Section, we developed a stochastic neural emulator that captures the joint evolution of the sea surface temperature (SST) field and the global mean net radiative flux at the top of the atmosphere (TOA) in the GFDL-CM4 climate model. Addressing a specific, well-posed problem, proved crucial in guiding the construction of the model: it enabled us to build on previous literature, restrict attention to just two variables and a limited range of spatial and temporal scales. These simplifications led to a stable emulator that responds to external forcing and can be used to investigate causal relationships via perturbation experiments. The model reconstruct the net TOA radiative flux when forced with a pre-computed SST trajectory. Beyond reconstruction, we illustrated that the model can be used to perform perturbation experiment, allowing us to enhance mechanistic understanding of the underlying physical processes. Findings are in qualitative agreement with results from traditional perturbation experiments in numerical models, giving additional confidence in the emulator's ability to capture key interactions across variables.

## V. CONCLUSIONS

In the first part of this paper, we addressed, at a pedagogical level, foundational issues in neural emulation of dynamical systems with climate applications in mind. We considered two scenarios: (i) when the full state vector is observed, and (ii) the more realistic case of partial observations. Our findings can be summarized as follows:

- i. *Fully observed state vector.* In this idealized case, it is possible to infer a dynamical model from data alone that reproduces the system’s stationary statistics and responds accurately to small, external perturbations.
- ii. *Partially observed state vector.* This more realistic case presents fundamental difficulties, even with access to high-quality data and powerful neural models architectures. The model skill now depends critically on two factors: (a) the choice of variables to model and (b) how unobserved degrees of freedom are parameterized.

These results highlight intrinsic limitations of purely data-driven modeling in high-dimensional systems, where the full set of relevant variables is typically unknown and there is no rigorous mathematical framework for selecting the proper variables to model. The identification of such variables, when possible, is inherently problem-dependent and often leads to adopting a coarse-grained representation of the dynamics. The next challenge is to parameterize the cumulative effect of unobserved degrees of freedom. This final step underscores that the issue of parameterization, traditionally associated with numerical modeling, is equally central to data-driven approaches using neural emulators. A promising perspective is to reconcile neural networks with principled modeling strategies, such as reduced-order modeling and stochastic parameterizations, by focusing on coarse-grained dynamics rather than constructing deterministic models that attempt to resolve as many spatiotemporal scales as possible.

In the second part of the paper, we built on these insights by constructing a stochastic neural emulator for the coarse-grained dynamics of sea surface temperature (SST) and net top-of-atmosphere (TOA) radiative flux. The model was trained on long unforced simulations of a coupled climate model and designed with a specific physical task in mind: capturing radiative feedbacks to SST anomalies. We showed that the emulator reproduces the stationary statistics of the system and, more importantly, allows us to reconstruct TOA radiative fluxes in forced simulations when provided with forced SST trajectories. To deepen this analysis, we applied linear response theory to extract the direct causal links between temperature modes and TOA fluxes, targeting the so-called “pattern effect” [29, 30]. These links, when projected back onto the high-dimensional state space, were found to be consistent with recent studies. This suggests that the emulator’s skill in reconstructing TOA fluxes under forcing arises for the right physical reasons. In this way, focusing on a few dominant modes, on a limited range of time scales, and using stochastic parametrizations allowed us to build a skillful and interpretable emulator.

Modeling real-world dynamical systems from data alone is severely constrained by high dimensionality and the fact that we typically observe only a subset of relevant variables [32, 40, 46]. This leads to the fundamental challenge of identifying, when possible, the proper variables to model, a problem recognized since the work of Onsager and Machlup (1953) [68] and highlighted in more recent studies [47, 48]. These challenges are especially pronounced in climate dynamics, where observations are always partial, and the underlying system is both high-dimensional and multiscale. In this context, the multiscale structure of the climate system can be an advantage, allowing us to model coarse-grained dynamics while treating unresolved processes stochastically. The need to formulate models tackling the effective dynamics of slow variables, rather than the full set of primitive equations, has a long history in climate science, even in non-data-driven settings where all governing equations are known. The early work of Charney and von Neumann, for example, demonstrated the conceptual and practical benefits of filtering out “meteorologically insignificant noise” and emphasized the need for interpretable and computationally efficient effective equations in meteorology [43, 44, 63, 123]. These insights remain broadly relevant when developing neural emulators, especially in future attempts of building atmosphere-ocean coupled emulators. In purely data-driven settings, focusing on stochastic models that target coarse-grained processes offers a promising way forward by reconciling rigorous approaches such as reduced-order modeling with the flexibility and power of neural networks. Possible strategies include learning stochastic parameterizations directly from data using deep learning (as in this paper), guiding variable selection through causal inference [124, 125], incorporating information theory and response theory into the training phase [56], studying the evolution of the climate system in its “latent” dynamics [65] (i.e. on the attractor) and incorporating empirical knowledge and physics constraints in the learning phase [7, 11, 25, 126]. Finally, the rather hard difficulty (at times irreducible) of data-driven modeling for the coupled atmosphere-ocean system can at times be ameliorated by building models tailored to solve specific problems, by building on prior literature and insights, and developed with a clear understanding of the relevant variables and the spatiotemporal scales at play.

## Appendix A: Technical and practical details on the model formulations

### 1. Multivariate data-driven stochastic models

Consider a  $N$ -dimensional dynamical system described by a stochastic differential equation  $d\mathbf{x} = \mathbf{f}(\mathbf{x})dt + \Sigma(\mathbf{x})d\mathbf{W}$ . This equation can be discretized by the forward Euler method as follows:

$$\Delta\mathbf{x} = \mathbf{x}(t + \Delta t) - \mathbf{x}(t) = \mathbf{f}(\mathbf{x}(t))\Delta t + \Sigma(\mathbf{x})\sqrt{\Delta t}\boldsymbol{\xi}(t) \quad (\text{A1})$$

where  $\boldsymbol{\xi}(t)$  is a Gaussian white noise with zero mean, unit variance, and  $\sqrt{\Delta t}\boldsymbol{\xi}(t)$  is the increment of the Wiener process  $\Delta\mathbf{W} = \mathbf{W}(t + \Delta t) - \mathbf{W}(t)$ . Without loss of generality, we rescale time units by the time sampling interval such that a non-dimensional time increment is  $\Delta t = 1$  [6–8, 127]. The strategy is then to fit a rescaled version of Eq. A1 from observational data alone. Such rescaled equation takes the following form:

$$\Delta\mathbf{x} = \mathbf{x}(t + 1) - \mathbf{x}(t) = \mathbf{f}(\mathbf{x}(t)) + \Sigma(\mathbf{x})\boldsymbol{\xi}(t). \quad (\text{A2})$$

We proceed in two steps:

- i. *Fitting the drift.* We compute  $\Delta\mathbf{x} = \mathbf{x}(t + 1) - \mathbf{x}(t)$  and fit the deterministic dynamics such that  $\Delta\mathbf{x} \approx \mathbf{f}(\mathbf{x}(t))$ . In the main paper, we considered two cases:

- *Linear drift.* In this case, given a trajectory  $\mathbf{x}(t) \in \mathbb{R}^N$ , we need to fit a matrix  $\mathbf{L} \in \mathbb{R}^{N,N}$  such that  $\Delta\mathbf{x} \approx \mathbf{L}\mathbf{x}(t)$  as close as possible. In practice, this is solved as a linear regression problem by minimizing the mean squared error. We use the linear regression module from the scikit-learn library [128].
- *Nonlinear drift.* We consider the following form:  $\Delta\mathbf{x} \approx \mathbf{f}(\mathbf{x}(t)) = \mathbf{L}\mathbf{x}(t) + \mathbf{n}(\mathbf{x}(t))$ , where  $\mathbf{L} \in \mathbb{R}^{N,N}$  is the linear operator and  $\mathbf{n}(\mathbf{x}(t))$  is the nonlinear operator parameterized by a multilayer perceptron (MLP). Both operators are fitted jointly by minimizing the mean squared error using a version of the gradient descent algorithm (Adam, [129]) with weight decay. The MLP considered here always consisted of one hidden layer. The number of neurons in the hidden layer depended on the application: we considered 30 neurons in the experiments with the triad model in Section III B 1 and 1000 neurons in the real-world application in Section IV. We played with more hidden layers but found a comparable performance, and sometimes a larger network also led to instabilities. The activation function used is the swish function (SiLU), which we found yields smoother responses to external perturbations. In contrast, the commonly used ReLU activation produced noisier responses. Furthermore, to ensure high accuracy in perturbation-response experiments, all data were processed using double-precision floating-point format.

- ii. *Fitting the stochastic term.* Having fitted the deterministic dynamics  $\mathbf{f}$ , we compute the residuals  $\mathbf{r}(t) \in \mathbb{R}^N$  as  $\mathbf{r}(t) = \Delta\mathbf{x} - \mathbf{f}(\mathbf{x}(t))$ . We then construct a suitable stochastic parametrization for this residual term. In the paper, we focus on two cases: additive and multiplicative noise.

- *Additive noise.* Given the residuals  $\mathbf{r}(t)$ , we proceed by computing their covariance matrix  $\mathbf{C} \in \mathbb{R}^{N,N}$  as  $\mathbf{C} = \langle \mathbf{r}\mathbf{r}^T \rangle$ , where brackets denote time averaging. We then consider the Cholesky decomposition of  $\mathbf{C}$  to derive a lower triangular matrix  $\Sigma \in \mathbb{R}^{N,N}$  such that  $\mathbf{C} = \Sigma\Sigma^T$ . The full fitted equation solved by the emulator can then be written as:

$$\mathbf{x}(t + 1) = \mathbf{x}(t) + \mathbf{f}(\mathbf{x}(t)) + \Sigma\boldsymbol{\xi}(t) \quad (\text{A3})$$

and we remind the reader that  $\boldsymbol{\xi}(t) \in \mathbb{R}^N$  is a Gaussian white noise with zero mean, unit variance.

- *Multiplicative noise.* Here, we consider state-dependent noise. To approximate it in a computationally efficient manner, we proceed as follows:
  - Given the residuals  $\mathbf{r}(t)$  at each time  $t$ , we compute their outer product  $\mathbf{C}(t) = \mathbf{r}(t)\mathbf{r}(t)^T$  which is a matrix of rank one.
  - We train a neural network predicting a lower triangular matrix  $\Sigma(\mathbf{x}(t))$  with positive diagonal, which can be interpreted as a Cholesky factor, such that  $\mathbf{C}(t) \approx \Sigma(\mathbf{x}(t))\Sigma(\mathbf{x}(t))^T$  as close as possible.

In practice, the loss function minimizes the mean squared error (MSE) between  $\mathbf{C}(t)$  and  $\Sigma(\mathbf{x}(t))\Sigma(\mathbf{x}(t))^T$  at each batch. A minimizer of the MSE loss approximates the conditional mathematical expectation  $\mathbb{E}[\mathbf{C}(t)|\mathbf{x}(t)]$ , that is the covariance matrix averaged over all residuals corresponding to the same state vector, as a function of this state vector, and can be seen as a generalization of a method presented in [130]

to multiple dimensions. The neural network architecture used here is identical to the one used for fitting the drift. The positivity of the diagonal terms of the lower triangular matrix  $\Sigma(\mathbf{x}(t))$  is enforced through a softplus activation function. Note that this (high-dimensional) multiplicative noise parametrization is only applied in the real-world-like case, where data are scarce: to prevent overfitting, we use early stopping during training, halting after only 5 epochs. The final fitted equation solved by the emulator is:

$$\mathbf{x}(t+1) = \mathbf{x}(t) + \mathbf{f}(\mathbf{x}(t)) + \Sigma(\mathbf{x}(t))\xi(t) \quad (\text{A4})$$

where again  $\xi(t) \in \mathbb{R}^N$  is a Gaussian white noise with zero mean, unit variance.

Furthermore, even in the real-world case of sea surface temperature fields and radiative fluxes, reducing the dimensionality to a few,  $N = 21$ , components led to a simplified computational problem where all neural networks could be trained on CPUs and on a personal computer.

## 2. Scalar data-driven stochastic models

Consider a trajectory of length  $T$  of a 1-dimensional dynamical system. As in the Section above, we assume that this scalar time series can be modeled as a discrete stochastic process with time-stepping  $\Delta t = 1$ , therefore rescaling our time-stepping by the sampling interval. The scalar equation we aim to fit is therefore:

$$\Delta x = x(t+1) - x(t) = f(x(t)) + \sigma(x)\xi(t). \quad (\text{A5})$$

The training of the deterministic (i.e. drift) dynamics follows exactly the same procedure of the multivariate case. Even the network considered are the same, with one hidden layer and 30 neurons. So we refer the reader to the Section above regarding the fitting of the deterministic dynamics and proceed in focusing on the stochastic case.

*Fitting the stochastic term.*

- *Additive noise.* We compute the residual time series  $r(t) = \Delta x - f(x(t))$  from the drift term. We then proceed in computing the standard deviation  $\sigma$  of such residual time series. The full fitted equation solved by the emulator can then be written as:

$$x(t+1) = x(t) + f(x(t)) + \sigma\xi(t) \quad (\text{A6})$$

and we remind the reader that  $\xi(t)$  is a scalar Gaussian white noise with zero mean, unit variance.

- *Multiplicative noise.* We again consider the residual time series  $r(t)$  from the drift term. We then compute at each time step  $t$  the square of the residual at that time step, i.e.  $r(t)^2$ . We then train a neural network to have  $g(x(t)) \approx r(t)^2$  by minimizing the mean squared error [130]. The neural network is again a MLP with one hidden layer with 30 neurons. Differently, from the neural networks considered for the drift, here we added a softplus activation function after the last layer of the network to ensure that the variance estimates are nonnegative. The final fitted equation solved by the emulator is:

$$x(t+1) = x(t) + f(x(t)) + \sqrt{g(x(t))}\xi(t). \quad (\text{A7})$$

## ACKNOWLEDGMENTS

Most of the ideas discussed in this work stem from collaborations and exchanges with colleagues and friends. I am grateful for the supportive and engaging environment of the Zanna Group at Courant, as well as for interactions within the broader M<sup>2</sup>Lines project. I thank Laure Zanna and Carlos Fernandez-Granda for their feedback during early stages of the project. I am especially grateful to Pasha Perezhogin, Rory Basinski, Chris Pedersen, and Andre Souza for their thoughtful feedback and for many enriching discussions on data-driven modeling of the Climate system. This work was supported in part through the NYU IT High Performance Computing resources, services, and staff expertise.

- 
- [1] M. Ghil and V. Lucarini, The physics of climate variability and climate change, *Rev. Mod. Phys.* **92**, 035002 (2020).
  - [2] V. Lucarini and M. Chekroun, Theoretical tools for understanding the climate crisis from Hasselmann’s programme and beyond, *Nat Rev Phys* (2023) (2023).
  - [3] C. Penland, Random Forcing and Forecasting Using Principal Oscillation Pattern Analysis, *Monthly Weather Review* **117**, 2165 (1989).
  - [4] C. Penland and P. Sardeshmukh, The optimal growth of tropical sea surface temperature anomalies, *Journal of Climate* **8**, 1999–2024 (1995).
  - [5] C. Penland, A stochastic model of indopacific sea surface temperature anomalies, *Physica D: Nonlinear Phenomena* **98**, 534 (1996), *nonlinear Phenomena in Ocean Dynamics*.
  - [6] S. Kravtsov, D. Kondrashov, and M. Ghil, Multilevel Regression Modeling of Nonlinear Processes: Derivation and Applications to Climatic Variability, *Journal of Climate* **18**, 4404–4424 (2005).
  - [7] D. Kondrashov, M. Chekroun, and M. Ghil, Data-driven non-markovian closure models, *Physica D: Nonlinear Phenomena* **297**, 33 (2015).
  - [8] K. Strouine, S. Kravtsov, D. Kondrashov, and M. Ghil, Reduced models of atmospheric low-frequency variability: Parameter estimation and comparative performance, *Physica D: Nonlinear Phenomena* **239**, 145 (2010).
  - [9] N. Agarwal, D. Kondrashov, P. Dueben, E. Ryzhov, and P. Berloff, A comparison of data-driven approaches to build low-dimensional ocean models, *Journal of Advances in Modeling Earth Systems* **13**, e2021MS002537 (2021).
  - [10] A. J. Majda and Y. Yuan, Fundamental limitations of ad hoc linear and quadratic multi-level regression models for physical systems, *Discrete and Continuous Dynamical Systems - Series B* **17**, 10.3934/dcdsb.2012.17.1333 (2012).
  - [11] A. Majda and J. Harlim, Physics constrained nonlinear regression models for time series, *NONLINEARITY* **26**, 201–217 (2013).
  - [12] A. Souza, Representing turbulent statistics with partitions of state space. part 1. theory and methodology., *J. Fluid Mech.* **997** (2024).
  - [13] A. Souza, Representing turbulent statistics with partitions of state space. part 2. the compressible euler equations., *J. Fluid Mech.* **997** (2024).
  - [14] L. T. Giorgini, A. N. Souza, and P. J. Schmid, Reduced markovian models of dynamical systems, *Physica D: Nonlinear Phenomena* **470**, 134393 (2024).
  - [15] L. Giorgini, Data-Driven Decomposition of Conservative and Non-Conservative Dynamics in Multiscale Systems, *Arxiv* <https://doi.org/10.48550/arXiv.2505.01895> (2025).
  - [16] J. Pathak, S. Subramanian, P. Harrington, S. Raja, A. Chattopadhyay, M. Mardani, T. Kurth, D. Hall, Z. Li, K. Aziz-zadenesheli, P. Hassanzadeh, K. Kashinath, and A. Anandkumar, FourCastNet: A Global Data-driven High-resolution Weather Model using Adaptive Fourier Neural Operators, *arXiv e-prints* 10.48550/arXiv.2202.11214 (2022), 2202.11214 [physics.ao-ph].
  - [17] R. Lam, A. Sanchez-Gonzalez, M. Willson, P. Wirnsberger, M. Fortunato, F. Alet, S. Ravuri, T. Ewalds, Z. Eaton-Rosen, W. Hu, A. Merose, S. Hoyer, G. Holland, O. Vinyals, J. Stott, A. Pritzel, S. Mohamed, and P. Battaglia, Learning skillful medium-range global weather forecasting, *Science* **382**, 1416 (2023), <https://www.science.org/doi/pdf/10.1126/science.adi2336>.
  - [18] K. Bi, L. Xie, H. Zhang, X. Chen, X. Gu, and Q. Tian, Accurate medium-range global weather forecasting with 3d neural networks, *Nature* **619**, 533–538 (2023).
  - [19] D. Kochkov, J. Yuval, I. Langmore, P. Norgaard, J. Smith, G. Mooers, M. Klöwer, J. Lottes, S. Rasp, P. Düben, S. Hatfield, P. Battaglia, A. Sanchez-Gonzalez, M. Willson, M. P. Brenner, and S. Hoyer, Neural general circulation models for weather and climate, *Nature* **632**, 1060–1066 (2024).
  - [20] O. Watt-Meyer, G. Dresdner, J. McGibbon, S. K. Clark, B. Henn, J. Duncan, N. D. Brenowitz, K. Kashinath, M. S. Pritchard, B. Bonev, M. E. Peters, and C. S. Bretherton, ACE: A fast, skillful learned global atmospheric model for climate prediction, *arXiv e-prints*, arXiv:2310.02074 (2023), arXiv:2310.02074 [physics.ao-ph].
  - [21] O. Watt-Meyer, B. Henn, J. McGibbon, S. K. Clark, A. Kwa, W. A. Perkins, and C. S. Bretherton, ACE2: Accurately learning subseasonal to decadal atmospheric variability and forced responses, *arXiv e-prints* <https://arxiv.org/abs/2411.11268> (2024).
  - [22] H. Guan, T. Arcomano, A. Chattopadhyay, and R. Maulik, LUCIE: A Lightweight Uncoupled CLimate Emulator with long-term stability and physical consistency for O(1000)-member ensembles, *arXiv* <https://doi.org/10.48550/arXiv.2405.16297> (2025).
  - [23] A. Chattopadhyay, M. Gray, T. Wu, and et al., Oceannet: a principled neural operator-based digital twin for regional oceans, *Sci. Rep.* **14**, 21181 (2024).
  - [24] S. Dheeshjith, A. Subel, A. Adcroft, J. Busecke, C. Fernandez-Granda, S. Gupta, and L. Zanna, Samudra: An AI global ocean emulator for climate., *Geophysical Research Letters* **52**, e2024GL114318 (2025).
  - [25] W. Chapman, J. Schreck, Y. Sha, D. Gagne II, D. Kimpara, L. Zanna, K. Mayer, and J. Berner, CAMulator: Fast Emulation of the Community Atmosphere Model, *Arxiv* <https://doi.org/10.48550/arXiv.2504.06007> (2025).
  - [26] C. Pedersen, L. Zanna, and J. Bruna, Thermalizer: Stable autoregressive neural emulation of spatiotemporal chaos, *Arxiv* <https://doi.org/10.48550/arXiv.2503.18731> (2025).
  - [27] R. Jiang, X. Zhang, K. Jakhar, P. Lu, P. Hassanzadeh, M. Maire, and R. Willett, Hierarchical Implicit Neural Emulators, *Arxiv* <https://doi.org/10.48550/arXiv.2506.04528> (2025).

- [28] S. Van Loon, M. Rugenstein, and E. A. Barnes, Reanalysis-based Global Radiative Response to Sea Surface Temperature Patterns: Evaluating the Ai2 Climate Emulator, Arxiv <https://doi.org/10.48550/arXiv.2502.10893> (2025).
- [29] J. Bloch-Johnson, M. A. A. Rugenstein, M. J. Alessi, C. Proistosescu, M. Zhao, B. Zhang, A. I. L. Williams, J. M. Gregory, J. Cole, Y. Dong, M. L. Duffy, S. M. Kang, and C. Zhou, The green's function model intercomparison project (gfmip) protocol, *Journal of Advances in Modeling Earth Systems* **16**, e2023MS003700 (2024), e2023MS003700 2023MS003700, <https://agupubs.onlinelibrary.wiley.com/doi/pdf/10.1029/2023MS003700>.
- [30] Y. Dong, C. Proistosescu, K. C. Armour, and D. S. Battisti, Attributing Historical and Future Evolution of Radiative Feedbacks to Regional Warming Patterns using a Green's Function Approach: The Preeminence of the Western Pacific, *Journal of Climate* **32**, 5471 (2019).
- [31] F. Ceconni, M. Cencini, M. Falcioni, and A. Vulpiani, Predicting the future from the past: An old problem from a modern perspective, *Am. J. Phys.* **11**, 1001–1008 (2012).
- [32] H. Hosni and A. Vulpiani, Forecasting in Light of Big Data, *Philos. Technol.* **31**, 557–569 (2018).
- [33] M. Baldovin, F. Ceconni, M. Cencini, A. Puglisi, and A. Vulpiani, The role of data in model building and prediction: A survey through examples, *Phys. Rev. Res.* **20**, doi:10.3390/e20100807 (2018).
- [34] A. Majda, C. Franzke, and D. Crommelin, Normal forms for reduced stochastic climate models, *Proc. Natl. Acad. Sci.* **10**, 3649–3653 (2010).
- [35] A. Majda, R. Abramov, and B. Gershgorin, High skill in low-frequency climate response through fluctuation dissipation theorems despite structural instability, *Proc. Natl. Acad. Sci.* **107**, 581–586 (2010).
- [36] A. Majda, B. Gershgorin, and Y. Yuan, Low-Frequency Climate Response and Fluctuation–Dissipation Theorems: Theory and Practice, *Journal of the Atmospheric Sciences* **67**, 1186–1201 (2010).
- [37] A. J. Majda, R. V. Abramov, and M. J. Grote, *Information Theory and Stochastics for Multiscale Nonlinear Systems* (CRM Monograph Series, American Mathematical Society, 2005).
- [38] U. Marconi, A. Puglisi, L. Rondoni, and A. Vulpiani, Fluctuation-dissipation: Response theory in statistical physics, *Phys. Rep.* **461** (2008).
- [39] A. Majda, C. Franzke, and K. Boualem, An applied mathematics perspective on stochastic modelling for climate, *Phil. Trans. R. Soc. A.* **366**, 2427–2453 (2008).
- [40] G. L. and A. Vulpiani, Prediction and Inference: From Models and Data to Artificial Intelligence, *Foundations of Physics* **54**, <https://doi.org/10.1007/s10701-024-00803-4> (2024).
- [41] A. Dalmedico, History and Epistemology of Models: Meteorology (1946–1963) as a Case Study., *Archive for History of Exact Science* **55**, 395–422 (2001).
- [42] L. A. Smith, What might we learn from climate forecasts?, *Proceedings of the National Academy of Sciences* **99**, 2487 (2002), <https://www.pnas.org/doi/pdf/10.1073/pnas.012580599>.
- [43] J. G. Charney, ON A PHYSICAL BASIS FOR NUMERICAL PREDICTION OF LARGE-SCALE MOTIONS IN THE ATMOSPHERE, *Journal of Meteorology* **6**, 372–385 (1949).
- [44] J. G. Charney, R. Fjörtoft, and J. Von Neumann, Numerical Integration of the Barotropic Vorticity Equation, *Tellus* **2** (1950).
- [45] F. Takens, Detecting strange attractors in turbulence, in *Dynamical Systems and Turbulence*, in *Lect. Notes in Mathematics*, Vol. 898, edited by D. Rand and L. Young (Springer, Berlin, Heidelberg, 1981) p. 21–48.
- [46] F. Ceconni, G. Costantini, C. Guardiani, M. Baldovin, and A. Vulpiani, Correlation, response and entropy approaches to allosteric behaviors: a critical comparison on the ubiquitin case, *Physical Biology* **5**, 056002 (2020).
- [47] M. Baldovin, F. Ceconni, and A. Vulpiani, Understanding causation via correlations and linear response theory, *Physical Review Research* **2**, 043436 (2020).
- [48] D. Lucente, A. Baldassarri, A. Puglisi, A. Vulpiani, and M. Viale, Inference of time irreversibility from incomplete information: Linear systems and its pitfalls, *Phys. Rev. Res.* **4**, 043103 (2022).
- [49] A. J. Majda, I. Timofeyev, and Vanden-Eijnden, Models for stochastic climate prediction, *Proc. Natl. Acad. Sci. USA* **96**, 14687–14691 (1999).
- [50] A. J. Majda, I. Timofeyev, and Vanden-Eijnden, A mathematical framework for stochastic climate models, *Proc. Natl. Acad. Sci. USA* **54**, 891–974 (2001).
- [51] K. Hasselmann, Stochastic climate models part i. theory., *Tellus* **28**, 473 (1976).
- [52] G. Lacorata and A. Vulpiani, Fluctuation-response relation and modeling in systems with fast and slow dynamics, *Nonlin. Processes Geophys.* **14**, 681–694 (2007).
- [53] B. Dubrulle, F. Daviaud, D. Faranda, L. Marié, and B. Saint-Michel, How many modes are needed to predict climate bifurcations? Lessons from an experiment, *Nonlin. Processes Geophys.* **29**, 17–35 (2022).
- [54] F. Falasca and A. Bracco, Exploring the Tropical Pacific Manifold in models and observations, *Phys. Rev. X* **12**, 021054 (2022).
- [55] I. Held, The Gap between Simulation and Understanding in Climate Modeling, *Bulletin of the American Meteorological Society*, 1609–1614 (2005).
- [56] A. Majda and D. Qi, Strategies for Reduced-Order Models for Predicting the Statistical Responses and Uncertainty Quantification in Complex Turbulent Dynamical Systems, *SIAM REVIEW* **60**, <https://doi.org/10.1137/16M1104664> (2018).
- [57] A. J. Majda, I. Timofeyev, and Vanden-Eijnden, A priori test of a stochastic mode reduction strategy, *Physica D* **170**, 206–252 (2002).
- [58] A. J. Majda, I. Timofeyev, and Vanden-Eijnden, Systematic strategies for stochastic mode reduction in climate, *J. Atmos. Sci.* **60**, 1705–1722 (2003).



- [59] T. J. O’Kane, D. Harries, and M. A. Collier, Bayesian structure learning for climate model evaluation, *Journal of Advances in Modeling Earth Systems* **16**, e2023MS004034 (2024).
- [60] J. Donges, Y. Zou, N. Marwan, and et al., Complex networks in climate dynamics, *Eur. Phys. J. Spec. Top.* **174**, 157–179 (2009).
- [61] I. Fountalis, C. Dovrolis, A. Bracco, B. Dilkina, and S. Keilholz,  $\delta$ -MAPS from spatio-temporal data to a weighted and lagged network between functional domain, *Appl. Netw. Sci.* **3**, 21 (2018).
- [62] F. Falasca, P. Perezhagin, and L. Zanna, Data-driven dimensionality reduction and causal inference for spatiotemporal climate fields, *Phys. Rev. E* **109**, 044202 (2024).
- [63] J. G. Charney, On the scale of atmospheric motions, *Geofysiske Publikasjoner* **17**, 1 (1948).
- [64] D. Crommelin and A. Majda, Strategies for Model Reduction: Comparing Different Optimal Bases, *Journal of the Atmospheric Sciences* **61**, 2206–2217 (2004).
- [65] H. Fan, B. Fei, P. Gentile, Y. Xiao, K. Chen, Y. Liu, Y. Qu, F. Ling, and L. Bai, Physically Consistent Global Atmospheric Data Assimilation with Machine Learning in a Latent Space, *Arxiv* <https://doi.org/10.48550/arXiv.2502.02884> (2025).
- [66] N. Lutsko, I. Held, and P. Zurita-Gotor, Applying the Fluctuation–Dissipation Theorem to a Two-Layer Model of Quasi-geostrophic Turbulence, *Journal of the Atmospheric Sciences* **72**, 3161–3177 (2015).
- [67] P. Hassanzadeh and Z. Kuang, The linear response function of an idealized atmosphere. part ii: Implications for the practical use of the fluctuation–dissipation theorem and the role of operator’s nonnormality, *Journal of The Atmospheric Science*, 3441–3452 (2016).
- [68] L. Onsager and S. Machlup, Fluctuations and irreversible processes, *Phys. Rev.* **91**, 1505 (1953).
- [69] M. Baldovin, A. Puglisi, and A. Vulpiani, Langevin equations from experimental data: The case of rotational diffusion in granular media, *PLoS ONE* **14**(2), e0212135 (2019).
- [70] C. Penland, M. D. Fowler, D. L. Jackson, and R. Cifelli, Forecasts of opportunity for northern california soil moisture, *Land* **10**, 10.3390/land10070713 (2021).
- [71] Y. Zhao and A. Capotondi, The role of the tropical Atlantic in tropical Pacific climate variability, *npj Clim Atmos Sci* **7** (2024).
- [72] J. Lien, Y.-N. Kuo, H. Ando, and S. Kido, Colored linear inverse model: A data-driven method for studying dynamical systems with temporally correlated stochasticity, *Phys. Rev. Res.* **7**, 023042 (2025).
- [73] J. Callahan, J.-C. Loiseau, G. Rigas, and S. Brunton, Nonlinear stochastic modeling with Langevin regression, *Proc. R. Soc. A* **477**:20210092, <https://doi.org/10.1098/rspa.2021.0092> (2021).
- [74] E. Lorenz, Deterministic nonperiodic flow, *J. Atmospheric Sci.* **20**, 130–141 (1963).
- [75] A. J. Linot, J. W. Burby, Q. Tang, P. Balaprakash, M. D. Graham, and R. Maulik, Stabilized neural ordinary differential equations for long-time forecasting of dynamical systems, *Journal of Computational Physics* **474**, 111838 (2023).
- [76] H. Risken, *The Fokker-Planck Equation – Methods of Solution and Applications* (Springer-Verlag, 1996).
- [77] J. Ismael, Reflections on the asymmetry of causation, *Interface Focus* **12**, 20220081 (2023).
- [78] E. Aurell and G. Del Ferraro, Causal analysis, correlation- response, and dynamic cavity, *J. of Phys.: Conference Series* **699**, 012002 (2016).
- [79] V. Lucarini, Revising and Extending the Linear Response Theory for Statistical Mechanical Systems: Evaluating Observables as Predictors and Predictands, *J Stat Phys* **173**, 1698–1721 (2018).
- [80] V. Lucarini and M. D. Chekroun, Detecting and attributing change in climate and complex systems: Foundations, green’s functions, and nonlinear fingerprints, *Phys. Rev. Lett.* **133**, 244201 (2024).
- [81] P. Castiglione, M. Falcioni, A. Lesne, and A. Vulpiani, *Chaos and coarse-graining in statistical mechanics* (Cambridge University Press, 2008).
- [82] C. Foias, G. R. Sell, and R. Temam, Inertial manifolds for nonlinear evolutionary equations, *Journal of Differential Equations* **73**, 309 (1988).
- [83] J. F. Gibson, J. Hacrow, and P. Cvitanović, Visualizing the geometry of state space in plane Couette flow, *Journal of Fluid Mechanics* **611**, 107–130 (2008).
- [84] X. Ding, H. Chaté, P. Cvitanović, E. Siminos, and K. A. Takeuchi, Estimating the Dimension of an Inertial Manifold from Unstable Periodic Orbits, *Phys. Rev. Lett.* **117**, 024101 (2016).
- [85] P. Cvitanović, R. Artuso, R. Mainieri, G. Tanner, and G. Vattay, *Chaos: Classical and Quantum* (Niels Bohr Inst., Copenhagen, 2016).
- [86] E. Altan, S. A. Solla, L. E. Miller, and E. J. Perreault, Estimating the dimensionality of the manifold underlying multi-electrode neural recordings, *PLOS COMPUTATIONAL BIOLOGY* **17**(11), 1 (2021).
- [87] E. D. Remington, S. W. Egger, D. Narain, J. Wang, and M. Jazayeri, A dynamical systems perspective on flexible motor timing, *Trends in Cognitive Sciences* **22**, 938 (2018), special Issue: Time in the Brain.
- [88] H. Sohn, D. Narain, N. Meirhaeghe, and M. Jazayeri, Bayesian computation through cortical latent dynamics, *Neuron* **103**, 934 (2019).
- [89] M. Jazayeri and S. Ostojic, Interpreting neural computations by examining intrinsic and embedding dimensionality of neural activity, *Current Opinion in Neurobiology* **70**, 113 (2021), computational Neuroscience.
- [90] M. Churchland, J. Cunningham, M. Kaufman, et al., Neural population dynamics during reaching, *Nature* **487**, 51–56 (2012).
- [91] G. Stephens, B. Johnson-Kerner, W. Bialek, and W. S. Ryu, Dimensionality and Dynamics in the Behavior of *C. elegans*, *PLoS Comput Biol* **4**, <https://doi.org/10.1371/journal.pcbi.1000028> (2020).
- [92] T. Ahamed, A. C. Costa, and G. Stephens, Capturing the continuous complexity of behaviour in *Caenorhabditis elegans*, *nature physics* (2020).

- [93] U. Cohen, S. Chung, D. Lee, *et al.*, Separability and geometry of object manifolds in deep neural networks, *Nature Communications* **11**, <https://doi.org/10.1038/s41467-020-14578-5> (2020).
- [94] C. Stephenson, suchismita padhy, A. Ganesh, Y. Hui, H. Tang, and S. Chung, On the geometry of generalization and memorization in deep neural networks, in *International Conference on Learning Representations* (2021).
- [95] M. Brunetti, J. Kasparian, and C. V  rard, Co-existing climate attractors in a coupled aquaplanet, *Clim Dyn* **53**, 6293–6308 (2019).
- [96] G. Margazoglou, T. Grafke, A. Laio, and V. Lucarini, Dynamical landscape and multistability of a climate mode, *Proc. R. Soc. A* **477**, <http://doi.org/10.1098/rspa.2021.0019> (2021).
- [97] C. Franzke and A. Majda, Low-order stochastic mode reduction for a prototype atmospheric GCM, *Journal of the Atmospheric Sciences* **2**, 457–479 (2006).
- [98] J. Berner and G. Branstator, Linear and nonlinear signatures in the planetary wave dynamics of an agcm: Probability density functions, *Journal of the Atmospheric Sciences* **64**, 117–136 (2007).
- [99] P. Sura, M. Newman, C. Penland, and P. Sardeshmukh, Multiplicative noise and non-Gaussianity: A paradigm for atmospheric regimes?, *Journal of Climate* **62**, 1391–1409 (2005).
- [100] H. Arnold, I. Moroz, and T. Palmer, Stochastic parametrizations and model uncertainty in the lorenz’ 96 system, *Phil Trans R Soc* **371**, 20110479 (2013).
- [101] A. Dawson and T. Palmer, Simulating weather regimes: impact of model resolution and stochastic parameterization, *Clim Dyn* **44**, 2177 (2015).
- [102] J. Berner and et al., Stochastic Parameterization: Toward a New View of Weather and Climate Models , *Bulletin of the American Meteorological Society* **98**, 565–588 (2017).
- [103] S. Hochreiter and J. Schmidhuber, Long short-term memory, *Neural Computation* **9**, 1735 (1997), <https://direct.mit.edu/neco/article-pdf/9/8/1735/813796/neco.1997.9.8.1735.pdf>.
- [104] B. Meyssignac, R. Guillaume-Castel, and R. Roca, Revisiting the Global Energy Budget Dynamics with a Multivariate Earth Energy Balance Model to Account for the Warming Pattern Effect , *Journal of Climate* **36**, 8113–8126 (2023).
- [105] F. Falasca, A. Basinski, L. Zanna, and M. Zhao, A fluctuation-dissipation theorem perspective on radiative responses to temperature perturbations, *Journal of Climate* **38**, 3239–3260 (2025).
- [106] J. J. Barsugli and P. D. Sardeshmukh, Global atmospheric sensitivity to tropical sst anomalies throughout the indo-pacific basin, *Journal of Climate* **15**, 3427 (2002).
- [107] C. Zhou, M. D. Zelinka, and S. A. Klein, Analyzing the dependence of global cloud feedback on the spatial pattern of sea surface temperature change with a green’s function approach, *Journal of Advances in Modeling Earth Systems* **9**, 2174 (2017), <https://agupubs.onlinelibrary.wiley.com/doi/pdf/10.1002/2017MS001096>.
- [108] B. Zhang, M. Zhao, and Z. Tan, Using a Green’s Function Approach to Diagnose the Pattern Effect in GFDL AM4 and CM4, *Journal of Climate* **36**, 1105 (2023).
- [109] Y. Dong, K. C. Armour, M. D. Zelinka, C. Proistosescu, D. S. Battisti, C. Zhou, and T. Andrews, Intermodel Spread in the Pattern Effect and Its Contribution to Climate Sensitivity in CMIP5 and CMIP6 Models, *Journal of Climate* **33**, 7755 (2020).
- [110] M. J. Alessi and M. A. Rugenstein, Surface temperature pattern scenarios suggest higher warming rates than current projections, *Geophysical Research Letters* **50**, e2023GL105795 (2023).
- [111] A. I. Williams, N. Jeevanjee, and J. Bloch-Johnson, Circus tents, convective thresholds, and the non-linear climate response to tropical ssts, *Geophysical Research Letters* **50**, e2022GL101499 (2023).
- [112] I. M. Held, H. Guo, A. Adcroft, J. P. Dunne, L. W. Horowitz, J. Krasting, and et al., Structure and performance of GFDL’s CM4.0 climate model, *Journal of Advances in Modeling Earth Systems* **11**, 3691–3727 (2019).
- [113] A. Adcroft, W. Anderson, V. Balaji, C. Blanton, M. Bushuk, C. O. Dufour, and et al., The GFDL global ocean and sea ice model OM4.0: Model description and simulation features, *Journal of Advances in Modeling Earth Systems* **11**, 3167–3211 (2019).
- [114] M. Zhao and Coauthors, The GFDL global atmosphere and land model AM4.0/LM4.0: 1. Simulation characteristics with prescribed SSTs., *Journal of Advances in Modeling Earth Systems* **10**, 691–734 (2018).
- [115] M. Zhao and Coauthors, The GFDL global atmosphere and land model am4.0/LM4.0: 2. Model description, sensitivity studies, and tuning strategies., *Journal of Advances in Modeling Earth Systems* **10**, 735–769 (2018).
- [116] R. T. Pierrehumbert, *Principles of Planetary Climate* (Cambridge University Press, 2010).
- [117] D. M. Romps, J. T. Seeley, and J. P. Edman, Why the forcing from carbon dioxide scales as the logarithm of its concentration, *Journal of Climate* **35**, 4027–4047 (2022).
- [118] M. Zhao, An investigation of the effective climate sensitivity in GFDL’s new climate models CM4.0 and SPEAR, *Journal of Climate* **35**, 5637–5660 (2022).
- [119] A. Timmermann and et al., El Ni  o-Southern Oscillation complexity, *Nature* **559**, 535 (2018).
- [120] S. M. Kang, P. Ceppi, Y. Yu, and I.-S. Kang, Recent global climate feedback controlled by southern ocean cooling, *Nature Geoscience* **16**, 775 (2023).
- [121] S. Van Loon, M. Rugenstein, and E. A. Barnes, Observation-based estimate of earth’s effective radiative forcing, *Proceedings of the National Academy of Sciences* **122**, e2425445122 (2025), <https://www.pnas.org/doi/pdf/10.1073/pnas.2425445122>.
- [122] E. Guilyardi, P. Braconnot, F.-F. Jin, S. T. Kim, M. Kolasinski, L. T., and I. Musat, Atmosphere Feedbacks during ENSO in a Coupled GCM with a Modified Atmospheric Convection Scheme, *Journal of Climate* **2**, 5698–5718 (2009).
- [123] J. G. Charney, The dynamics of long waves in a baroclinic westerly current, *Journal of the atmospheric sciences* **4**, 136–162 (1947).

- [124] F. Iglesias-Suarez, P. Gentine, B. Solino-Fernandez, T. Beucler, M. Pritchard, J. Runge, and V. Eyring, Causally-informed deep learning to improve climate models and projections, *Journal of Geophysical Research: Atmospheres* **129**, e2023JD039202 (2024).
- [125] N. Chen and H. Liu, Minimum reduced-order models via causal inference, *Nonlinear Dyn* **113**, 11327–11351 (2025).
- [126] T. Beucler, M. Pritchard, S. Rasp, J. Ott, P. Baldi, and P. Gentine, Enforcing analytic constraints in neural networks emulating physical systems, *Phys. Rev. Lett.* **126**, 098302 (2021).
- [127] S. Kravtsov, M. Ghil, and D. Kondrashov, Empirical Model Reduction and the Modeling Hierarchy in Climate Dynamics and the Geosciences, in *Stochastic Physics and Climate Modeling*, edited by T. Palmer and P. Williams (Cambridge University Press, 2009) pp. 35–72.
- [128] F. Pedregosa, G. Varoquaux, A. Gramfort, V. Michel, B. Thirion, O. Grisel, M. Blondel, P. Prettenhofer, R. Weiss, V. Dubourg, J. Vanderplas, A. Passos, D. Cournapeau, M. Brucher, M. Perrot, and E. Duchesnay, Scikit-learn: Machine learning in Python, *Journal of Machine Learning Research* **12**, 2825 (2011).
- [129] D. P. Kingma and J. Ba, Adam: A method for stochastic optimization, arXiv preprint arXiv:1412.6980 (2014).
- [130] J. Adler and O. Öktem, Deep bayesian inversion, arXiv preprint arXiv:1811.05910 **1**, 7 (2018).